New-generation 3D Printed Biomedical Device Based on Micro-scale Hydrodynamic Cavitation

By

Seyedali Seyedmirzaei Sarraf

Submitted to the Graduate School of Natural Science and Engineering In partial fulfillment of the requirement for the degree of Master of Science

Sabanci University

July 2022

New-generation 3D printed biomedical device based on micro-scale hydrodynamic cavitation

APPROVED BY:

DATE OF APPROVAL: 06/07/2022

ABSTRACT

New-generation 3D printed biomedical device based on micro-scale hydrodynamic cavitation

Seyedali Seyedmirzaei Sarraf

M.Sc. Thesis, July 2022

Advisor: Dr. Morteza Ghorbani
Co-Advisor: Prof. Ali Koşar

Keywords: Biomedical Instrument, Hydrodynamic Cavitation, Flexible Cystoscopy Probe, Additive Manufacturing, *In vivo* Experiment

Cavitation is a phase change phenomenon from liquid phase to vapor phase upon a sudden drop in local pressure below the saturation vapor pressure. Energy of nucleation sites is stored inside cavitation bubbles and transferred with it. The collapse of cavitation bubbles as a result of this phenomenon releases a large amount of energy and has mechanical, thermal, and chemical effects on the nearby surface. As a biomedical application, laser and acoustic induced cavitation accounting for two important types of cavitation have been extensively used for treatment of urinary tract disorders which requires ablation procedures. The complexity of such devices leads to increased final production cost of devices. On the other hand, hydrodynamic cavitation could be an inexpensive, local and energy efficient alternative and has also been previously proven through *in vitro* trials. In this thesis, a portable flexible cystoscopy device equipped with a hydrodynamic cavitation probe was designed, fabricated, and examined successfully in an *in vivo* test. The related pathology report indicated that sharply demarcated tissue defects occurred in the epithelial and subepithelial tissues in the area exposed to the hydrodynamic cavitation. As a result, a new-generation biomedical device prototype based on micro-scale hydrodynamic cavitation was designed and developed.

ÖZET

Mikro ölçekli hidrodinamik kavitasyona dayalı yeni nesil 3D baskılı biyomedikal cihaz

Seyedali Seyedmirzaei Sarraf

Yüksek Lisans Tezi, Temmuz 2022

Danışman: Dr. Morteza Ghorbani
Yardımcı Danışman: Prof. Ali Koşar

Anahtar Kelimeler: Biyomedikal Enstrüman, Hidrodinamik Kavitasyon, Esnek Sistoskopi Probu, Eklemeli İmalat, *In vivo* Deney

Kavitasyon, yerel basıncın doymuş buhar basıncının altına düşmesiyle sıvı fazdan buhar fazına geçiş olayıdır. Çekirdeklenme bölgelerinin enerjisi, kavitasyon kabarcıklarının içinde depolanır ve onunla birlikte aktarılır. Bu fenomenin bir sonucu olarak kavitasyon kabarcıklarının çökmesi, büyük miktarda enerji açığa çıkarır ve yakındaki yüzey üzerinde mekanik, termal ve kimyasal etkilere sahiptir. Biyomedikal bir uygulama olarak, iki önemli kavitasyon tipini hesaba katan lazer ve akustik kaynaklı kavitasyon, ablasyon prosedürleri gerektiren idrar yolu bozukluklarının tedavisinde yaygın olarak kullanılmaktadır. Bu tür cihazların karmaşıklığı, cihazların nihai üretim maliyetinin artmasına neden olur. Öte yandan, hidrodinamik kavitasyon ucuz, yerel ve enerji açısından verimli bir alternatif olabilir ve daha önce in vitro deneylerle kanıtlanmıştır. Bu tezde, bir hidrodinamik kavitasyon probu ile donatılmış taşınabilir bir esnek sistoskopi cihazı tasarlanmış, üretilmiş ve bir in vivo testte başarılı bir şekilde incelenmiştir. İlgili patoloji raporu, hidrodinamik kavitasyona maruz kalan bölgedeki epitel ve subepitelyal dokularda keskin sınırlı doku defektlerinin oluştuğunu gösterdi. Sonuç olarak, mikro ölçekli hidrodinamik kavitasyona dayalı yeni nesil biyomedikal cihaz prototipi tasarlanmış ve geliştirilmiştir.

ACKNOWLEDGEMENTS

I would like to thank my beloved family, especially my wife, for their unconditional support throughout my graduate education.

I want to thank Professor Ali Koşar and Dr. Morteza Ghorbani for providing their support and sharing their valuable knowledge during my studies.

I want to thank Dr. Huseyin Uvet, Dr. Ozlem Kutlu, and Dr. Meral Yuce for kindly accepting my invitation in becoming my thesis defense's jury members.

I would like to thank all my group members especially Ilayda Namli, and my other collaborators Özcan Kanbur, Ezgi Kestek.

This work was supported by TUBITAK (The Scientific and Technological Research Council of Turkey) Support Program for Scientific and Technological Research Project (Grant Nos. 118S040). Support from the Sabanci University for the FENS Conference Travel Grant is acknowledged, and the equipment utilization of the Sabanci University Nanotechnology Research and Applications Center (SUNUM) is gratefully appreciated.

Table of Contents

List of Tables

List of Figures

1. CHAPTER ONE: INTRODUCTION

1.1. Background

Current gold standard medical approaches for treatment of urinary tract disorders have become popular methods as they mostly offer extracorporeal and noninvasive treatment possibilities. Although it is important to facilitate comminution for the disorders including kidney stones, bladder stones, and ablation of abnormal tissues such as polyps as well as benign prostate hyperplasic tissues, tissue injury must be prevented as well. Current treatment methods are based on cavitation bubble generation and collapse by setting up a tension (acoustic cavitation) or depositing an energy (laser or optic cavitation) into the medium, which mostly works in complex and expensive devices. However, micro-scale hydrodynamic cavitation as an energy efficient, local, and inexpensive alternative method has been recently studied in *in vitro* experiments and the potential of this approach has been revealed in treatment of abovementioned disorders. Therefore, there is a possibility to further investigate the performance of micro-scale hydrodynamic cavitation for tissue ablation in *in vivo* tests and to develop a new generation biomedical device prototype, which constitutes the motivation of this thesis.

1.1.1. Fundamentals of cavitation

Cavitation is a phase change phenomenon in response to a sudden decrease in the local pressure of a fluid below the saturation vapor pressure. This phenomenon requires an input energy to dissociate intermolecular bonds within the fluid followed by the formation of bubbles (1). Cavitation could be induced by using two general approaches: tension-based and energy deposition-based methods (2). The driving force of tension-based methods depends on the presence of a low-pressure region/wave within the fluid domain, while the energy deposition-based methods require the focus of optical or electrical energy into the fluid to excite and enlarge submicron bubbles by generating plasma and heat. Hydrodynamic and acoustic cavitation are categorized in the former group (tension-based), while the latter group encompasses electrical discharge and laser induced techniques. Cavitation phenomenon represents a three-step cyclic behavior of inception, growth/oscillation, and collapse. The inception of cavitation bubbles initiates with

nucleation, which is a self-organized process leading to the formation of new thermodynamic phases. Nucleation and evolution of generated nuclei are affected by various parameters such as excitation method, fluid properties, contaminants and impurities, residence time, surface characteristics of the fluid-solid interface and confining geometry. During the growth, phase energy is deposited into the bubble, which is released while imploding by means of sound or light or heat (3). Collapse of an evolved bubble happens precipitately leading to light emission (luminescence), shockwaves, very high localized pressures and temperatures (4,5). In addition, physio-chemical effects of violent bubble implosion in the vicinity of a rigid body or surface encompass formation of microjet flows near the surfaces, enhanced mixing at the vicinity of collapse zone, and production of chemical species (6–8).

Undesired energy release of collapsing cavitation bubbles leads to some technological problems such as corrosion in ships' propellers, destabilizing liquid propellent rockets, and lysing red blood cells at artificial heart valves (9). However, the idea of carefully harnessing the collapse energy has opened new lanes in cavitation related studies to consider the possibility of exploiting the released energy as a constructive effect in many areas including chemical (10), wastewater treatment (11), cleaning (12), and biomedical applications (13). To this end, incorporating cavitation with microfluidic technologies presents unique superiorities over conventional scale practices in terms of reduced required amount of liquid, enhanced monitoring, and real-time analyzing, as well as improved control and manipulation over nucleation sites and bubble dynamics. Under suitable conditions, any fluid inside microfluidic devices is susceptible to the formation of cavitation. In 2001, this phenomenon was first analyzed in a microfabricated turbopump blade on micro-scale (14). Spatial confinement of cavitation sites affects the nucleation and evolution of cavitation bubbles on micro-scale. Mishra and Peles (15,16) conducted the first comprehensive study on hydrodynamic cavitation in microfluidic systems in 2005. Their findings revealed the similarities and differences of cavitation inception on micro- and macro-scale. They indicated that the size effect is dominant on micro-scale, and since nuclei have small residence time for growth, liquid could tolerate lower pressures in comparison with macro-scale.

Cavitation bubbles have received much interest in bio-related applications (17). Understanding the spatiotemporal behavior of these bubbles as well as their mechanical, thermal, and chemical effects in interactions with biological entities or inside bio-related

processes is, therefore, critical for designing reliable miniature devices. Despite the progress in conventional scale experimental techniques, precise local measurement of complex behavior of cavitating flows in small spatial and temporal scales is still challenging (18). Numerical studies serve as an appropriate complement to the experimental studies since they can provide more details and insights about cavitation physics, which cannot be obtained easily with experiments. On the other hand, lab-on-a-chip devices provide a platform for researchers to conduct smart and rigorous experiments under well-controlled conditions. Therefore, hydrodynamically/optically/acoustically induced cavitation on lab-on-chips have been investigated to evaluate cell-bubble interaction and cavitation impact on biological substances. A detailed review on the fundamentals and biomedical applications of micro-scale cavitation is provided in (19) by the author of the current thesis.

1.1.1.1. Nucleation

Microfluidic devices have a length scale between 1-1000 micrometers, which are 10^3-10^4 times smaller than conventional counterparts. The recent advances in the semiconductor-based systems led to the fluid flow velocities up to 20-200 m/s (20–23) in microfluidic devices. In this regard, cavitation occurs through these devices by providing the appropriate hydrodynamic conditions.

Geometry, flow dimensionless parameters, nuclei sources, surface roughness and chemistry, which play important roles in large-scale systems, have been altered on micro-scale due to limitations in fabrication methods and material selection (24). Regardless of fluid temperature, among these parameters, the nuclei sources have a significant role in the inception and development of micro-scale cavitation (25). The device geometry, surface properties, and micro-scale flow behavior are the parameters affecting the nucleation mechanism in the microfluidic systems. The term “nuclei” refers to the contaminants and interfaces in the liquid that generate weak points, where rupture of liquid occurs (26). Cavitation, as a nonequilibrium phenomenon, has no exact theoretical explanation. In order to provide a theoretical description of this phenomenon, many research efforts have been focused to explain how likely it is for nuclei to form cavities in a negative pressure zone in the bulk liquid for the ambient temperature and liquid surface tension using the Classical Nucleation Theory (27) (CNT). The nucleation term refers to the conditions under which the systems reach the nonequilibrium metastable

state. Cavitation occurs when the liquid is under a negative pressure, at which the fluid becomes thermodynamically unstable and finally reaches the metastable state, where the phase separation will eventually result in the formation of small bubbles, which are called nuclei (28). Metastability (supersaturated vapor) is a local minimum of free energy as a function of the appropriate order parameter (29). According to the classical nucleation theory, the formation and subsequent growth of a bubble would be an 'activated event' only when the source nuclei is at the critical radius and surpasses the free energy barrier allowing it to grow to a macroscopic size. Fisher(30) presented the study "The Fracture of Liquids" in 1948, where the rate of bubble formation was calculated with the CNT for water under the negative pressure. In the metastable stage, the amount of the energy barrier is simply defined as a function of the liquid-vapor surface tension and liquid pressure (31). Surface tension is strongly dependent on the liquid property-cohesivity, defined as the metastability degree. For instance, water is a strongly cohesive liquid due to hydrogen bonding and has an unusually high surface tension compared to other liquids, which leads to a high degree of metastability or high energy barrier (32).

Bubble nucleation refers to the initialization of the phase transition from liquid to vapor. Nucleation is categorized into heterogeneous and homogeneous nucleation based on the location, where nucleation occurs. Heterogeneous nucleation is a ubiquitous mechanism initiating the phase change (33). In heterogeneous nucleation, the solid walls and existing impurities have an indispensable role, which causes a reduction in the required activation energy for triggering the phase transition and forming a new thermodynamic phase. The surface topology plays a significant role in reducing or increasing the fluid tensile strength. For example, the surface hydrophobicity or existence of the conical cavity (on the surface) causes a reduced local tensile strength and leads to heterogeneous nucleation. In addition to surface topology, the possibility of the existence of a gas packet at the solid surface can initiate heterogeneous cavitation. This model is known as the crevice model (34). According to this model, small gas pockets on microscopic scale are stabilized at the bottom of cracks or crevices located on hydrophobic solid impurities. Strasberg (35) presented an experimental study on ultrasonic cavitation in tap water and applied this theoretical model to reveal the effect of trapped gas packets on the cavitation inception pressure. Atchley and Prosperetti (36) parametrically investigated this model with an experimental study. They presented new conditions and approach for applying this model in different AC experiments. In this model, gas-diffusion effect was neglected (29).

Therefore, it would be more suitable for AC studies than HC studies (36). Mørch(37) conducted a comprehensive study on this model to cover the existing conflicts in the literature. In this study, a new applicable model for the calculation of critical pressure of skin-covered free gas packets was proposed.

Homogeneous nucleation happens within the bulk fluid (1). The homogeneous nucleation and classical nucleation theory are extensively used in cavitation studies (38). It is reasonable to assume that within the pure liquid, homogeneous nucleation requires a higher supersaturation level than heterogeneous nucleation because there is no auxiliary parameter to decrease the tensile strength unlike in heterogeneous nucleation (26,33). Homogenous nucleation on micro-scale is described by scaling down the liquid surface tension to the microscopic size of bubbles of few micrometer sizes. According to the homogeneous nucleation theory, the cavity generates and grows when the bulk liquid pressure is slightly less than the liquid saturation at the local nucleation site. Cavitation on micro-scale is associated with high velocity flows (100-200 m/s) (39–41). With such a high velocity and system size, the dwell-time of a nucleus in the low-pressure zone diminishes. Thus, a nucleus does have any sufficient time to grow and become active. It is worth mentioning that the homogenous nucleation mechanism does not have a dominant role on micro-scale cavitation (23,24,42,43).

1.1.1.2. Evolution and Flow Patterns

Hydrodynamic cavitation in microfluidic devices occurs when the fluid flow experiences a considerable static pressure drop when it passes through a flow restrictive element inside a microchannel. In this regard, different geometries (micro-orifices (15), micro-venturis (20,44), micro-diaphragms (20,44), micro-pillar (45), micro-steps (39)), functional surfaces (hydrophilic or hydrophobic (43), roughen or patterned (46)), working fluids (isotropic or anisotropic (47), pure or impure (20,48), mixtures (49)) were utilized to characterize various micro-scale cavitation flow patterns. In a pioneering study, Mishra *et al.* (15) developed the first microfluidic device to study micro-scale cavitation using water as the working fluid. Their device was a micro-orifice with a width of 11.5 μm embedded in a micro-channel with a width of 100.2 μm and depth of 101.3 μm. In their study, they were able to study different micro-scale cavitating flow regimes by altering the inlet and outlet pressure boundary conditions. At a critical pressure value above the vapor pressure, they reported the formation of gaseous cavitation originating from the

growth of nuclei of dissolved gasses. By reducing the static pressure in the 'Vena Contracta' region, vapor cavity formation was observed. Further reduction in the outlet pressure beyond a certain value did not change the flowrate because of the formation of choked flow, where the cavitation cloud elongated through the channel, which was called as the supercavitation flow pattern. They concluded that in contrast to macro-scale cavitation, the existence of dominant size scale effect on micro-scale increased the metastability of the fluid, which led to a reduced incipient cavitation number. In addition, cavitation under choked flow conditions was not dependent on any pressure or velocity effect but relied on the heterogeneity of the fluid and device. The other reported deviation of micro-scale cavitation from macro-scale cavitation was the fast transition from bubbly flow to choked flow followed by supercavitation. Moreover, a considerable inception and desinent cavitation hysteresis was observed for micro-scale cavitation. In another study, Medrano *et. al.* (20) investigated micro-scale hydrodynamic cavitation through micro-diaphragm and micro-venturi structures by scrutinizing deionized water with and without the presence of nano-aggregated particles. They concluded that in the case of pure deionized water, the onset of cavitation was delayed due to the metastability of the liquid on micro-scale, and the presence of nanoparticles with the lowest concentration threshold only affected cavitation inception for the micro-diaphragm configuration.

In the study of macro-scale cavitation flow patterns behind a bluff body by Matsudaira *et al.* (50), it was reported that there existed three different cavitating flow patterns including cyclic cavity pattern, where vapor bubbles were shed in the wake region, fixed cavity pattern, where the vapor pocket sticked to the body, and transition cavity pattern, where both fixed and cyclic cavity patterns appeared. In another study, Nayebzadeh *et al.* (45) investigated cavitating flow patterns on micro-scale behind a circular micro-pillar and observed shed vapor bubble, rotational vapor region in the vicinity of the pillar, attached cavity, and persistent elongated attached cavity. They concluded that the main difference between macro and micro-scale cavitation was the absence of the transition cavity pattern in the evolution of different patterns of micro-scale hydrodynamic cavitation for a micro-pillar configuration. Ghorbani *et al.* (48) studied micro-scale cavitating flow patterns in a micro-orifice configuration for both pure water and water containing poly vinyl alcohol (PVA) microbubbles. They used three separate microfluidic devices having different surface modifications, which included structural sidewall roughness, surface roughness and plane surface. They reported the formation of attached twin cavities at the inlet of the

micro-orifice as the first observed pattern and described the cavitating flow evolution with increasing the upstream pressure as the separation reattachment of the first pattern followed by the fully developed cavitation pattern and finally the supercavitation pattern. They concluded that the transition from inception to supercavitation happened faster compared to other cases with the use of PVA microbubbles and structural sidewall roughness. In another experimental study conducted by the same group, the optimum device geometry for a micro-orifice configuration with sidewall roughness was investigated in order to attain the most facile cavitation generating configuration (51). The aim was to characterize flow patterns and to provide an understanding about the size effect of the configuration on development of flow patterns from cavitation inception to supercavitation on micro-scale. In that study, different hydraulic diameters and lengths of microchannels as well as the structural sidewall roughness with diverse sizes were considered. In another study, Hosseinpour *et al.* (41) investigated flow patterns on micro-scale cavitating flows inside a microfluidic device containing eight parallel micro-orifices with sidewall roughness. They reported that their presented microfluidic device was able to generate different cavitating flow patterns simultaneously inside the same chip. The observed flow patterns included cavitation clouds, bubbly flow, attached and detached cavitating flows as well as sheet cavity. Podbevšek *et. al.*(52) explored the possibility of the formation of supercavitation inside a microfluidic device with the configuration of a micro-Venturi. They found that the formation of the supercavitation pattern was hindered as a result of the generation of the Kelvin-Helmholtz instability. The evolved cavitation flow pattern compromised single attached cavitation cloud, spatially followed by the zone, where the Kelvin-Helmholtz instability occurred, and finally the region, where the shed small cavities existed.

1.1.1.3. Collapse

When a nucleus evolves through a phase change from liquid to vapor, an amount of energy pertinent to the latent heat is deposited into the bubble cooling the surrounding fluid in the vicinity of the vapor cavity. Inversely, at the time of collapse, this energy is released by heating the nearby fluid (39). Liquid type and temperature are determining parameters for the presence of this effect. In this regard, Ayela *et. al.* (53) investigated thermal mapping of the temperature gradients due to thermal effects of micro-scale cavitation. They were able to analyze this phenomenon by combining a confocal

microscopy to a microfluidic device capable of generating hydrodynamic cavitating flows, where the tested fluid was deionized water seeded with thermosensitive nanoprobes. They reported an enhanced intensity of thermal gap on micro-scale. When thermal effects are negligible, bubble collapse happens vigorously causing high interface velocities and localized pressures. A generated submerged single bubble cavity experiences multiple cycles involving growth-collapse-rebound, where the first two-three cycles differ from the rest. By electrical discharge excitation of a single bubble, Buogo *et al.*(54) observed that just for the first three growth-collapse cycles the implosion happened at the end of each cycle, and an oscillating regime existed for later cycles. Considering that the liquid temperature affects the vapor pressure, they explained that the difference in the behavior of the collapsing and oscillating cycles stems from the fact that the time lapse for the first two-three cycles provides the required time for the bubble to cool down from the initially induced temperature to the surrounding liquid temperature levels, causing a reduction in the responsive compression pressure. For a single spherical cavitation bubble, the amount of stored potential energy, E_b, within the bubble could be estimated as (55):

$$E_b = \frac{4}{3}\pi p_\infty R_{max}^3 = \eta E_{dis}$$

where the discharge energy of the bubble, E_{dis}, is corelated to the stored potential energy of the bubble, E_b, with the discharge ratio of η. Several studies were conducted to reveal the relationship between vapor and ambient pressures with the discharge ratio (55–58). The discharge energy in a growth-collapse-rebound cycle of a single bubble, which contains gas/vapor mixture, is emitted as acoustic waves, where the amount of emitted energy is equal to the difference between the potential energy of the initial bubble at its maximum radius and the potential energy of the rebounded bubble at its peak size (54). Sato *et al.* (59) scrutinized the formation of hydrogen while generating laser and electrical discharge induced cavitation in water and proposed a relationship of the produced hydrogen mass with the potential energy of the bubble. They stated that the amount of hydrogen, which was produced due to the thermal dissociation of the laser and electrical discharges at the beginning of the experiment, was proportional to the amount of rebound potential energy of the bubble. The presence of non-condensable gas inside a vaporous cavity substantially alters the bubble dynamics and collapse behavior. In this regard, Prosperetti (60) studied the speed of sound for a bubbly liquid comprised of gas-vapor

cavities. In addition, bubble dynamics and collapse near the rigid surfaces are the other topics of interest. To this end, Blake *et. al.* (61) developed a fundamental principle, Kelvin impulse, providing a physical insight into bubble dynamics and collapse near boundaries. The implosion of a bubble near a rigid boundary causes the impact of a liquid jet as well as the impingement of shockwaves on the boundary (62). These characteristics make cavitation a suitable method for cleaning applications (12,63). The other important issue is the lifetime of a bubble, which is directly related to its size. It has been reported that the existence of microbubbles (1-1000 microns) lasts in the order of seconds, while it is in the order of minutes for macro-bubbles (>1mm). Surprisingly, nanoscale bubbles (with a mean diameter of 100-200 nanometers) have an extraordinary lifetime of several weeks (64,65).

1.1.1.4. Luminescence and Chemiluminescence

Cavitation bubbles emit light under certain conditions, where they experience nonlinear oscillations or rapid adiabatic implosions. Conversion of sound to light by focusing the diffused energy of acoustic waves into oscillating bubbles is called sonoluminescence. The analysis of the emitted light using spectroscopic, and plasma diagnostic tools revealed the presence of localized extreme conditions of temperatures up to 20000 K and pressures in the order of several thousand bars inside a cold liquid (3). Such conditions could trigger chemical reactions by production of H and OH radicals. Chemiluminescence of luminol is a well-known method of monitoring the formation of these radicals through observing the emitted photons (66). Considering micro-scale cavitation induced with acoustic fields, for bubbles confined inside the boundaries of microfluidic devices, there are several challenges in focusing the sound energy into bubbles because of the instabilities and viscous force, which hinder the nonlinear oscillation of bubbles by reducing the wall speed. To this end, Tandiono *et al.* (67) studied the presence of sonoluminescence and chemiluminescence within a polydimethylsiloxane (PDMS) based microfluidic devices exposing a slug flow to an acoustic field. They reported the formation of OH radicals in micro-scale indicating a faster decay rate compared to that of macro-scale condition. According to their findings, the advantage of micro-scale OH production is the spatial control over the chemical reactions offered by lab o-a chip devices. Also, they realized the generation of sonoluminescence at micro-scale pointing out a considerably lower photon yield compared to chemiluminescence. Another

remarkable observation was that chemiluminescence did not terminate right after switching the sound source off, which was the case for sonoluminescence. The production of reactive oxygen species (ROS) through hydrodynamic cavitation due to its high flow rates is an active area of research in wastewater treatment applications as advanced oxidation processes (AOPs) (10,11). However, in large-scale, it is not simple to analyze the chemical reactions induced by hydrodynamic cavitation. Exploiting the advantage of lab on-a chip devices, Podbevsek *et. al.* (68) observed the hydrodynamic cavitation induced chemiluminescence of production of ROS in a transparent microfluidic chip and corelated the yield of emitted photons with the total flow rate and pressure drop. In another study from the same group, a framework was proposed to map the location and quantify the free radical yield of hydrodynamic cavitation induced ROS production inside a microfluidic chip (69). This study is important because it offers an ‘’*in situ*’’ approach to optimize microreactors employing hydrodynamic cavitation. Studies addressing the luminescence of hydrodynamic cavitation in micro-scale are limited, and more research efforts are required to shed light on this field. In another study, Perrin *et. al.* (70) measured and compared luminescence of deionized water and chemiluminescence of an alkaline luminol solution for matching hydrodynamic flow regimes in a micro-step cavitating chip by a novel experimental setup capable of detecting low intensity photons inside a light tight box.

1.1.2. Biomedical Applications of Micro-scale Hydrodynamic Cavitation

For the first time Koşar *et. al.* (71) investigated the effectiveness of bubbly cavitating flow on the erosion of chalk specimens mimicking the renal calculi as well as its impact on destroying leukemia/lymphoma cells exploiting micro-scale orifice throat experimentally. Later, Perk *et. al.* (72) studied the erosion rate of the calcium oxalate kidney stone samples exposed to micro-scale hydrodynamic cavitating flow with a similar experimental device and reported the 0.31 mg/min erosion rate for renal calculi samples. In accordance with the reported studies, Itah *et. al.* (73) scrutinized the consequence of the hydrodynamic bubbly cavitating flow on prostate cells and benign prostatic hyperplasia tissue and concluded that this approach is comparable with ultrasonic cavitation method in ablation of aberrant pathological tissues. In another experimental study, Uzusen *et. al.* (74) investigated the effect of hydrodynamic orifice throat distance

to kidney stone specimen on erosion rate. They proposed a correlation for the erosion rate of renal calculi as a function of time, distance, and properties of the material. Ghorbani *et. al.* (75) reviewed the lithotripsy and cavitation-based methods used in kidney stone treatment and emphasized the hydrodynamic cavitation as an alternative to ultrasound induce cavitation techniques in kidney stone therapy. Sozer *et. al.* (76) and Ghorbani *et. al.* (77) designed and prototyped a multi segmented flexible cystoscopy probe with the outer diameter of 10 mm comprising of a medical camera and a hydrodynamic cavitation nozzle. Gevari *et. al.* (78) analyzed the mechanical deformation of different cancer cell lines exposed to cavitating flows and discussed their various responses to cavitation bubbles. Abbasi *et. al.* (79) designed and prototyped a continuum flexible cystoscopy device equipped with small-scale hydrodynamic cavitation nozzle and tested its efficiency in ablating prostate cancer tissue in an *in vitro* test. They reported the capability of the cavitating flow in destroying the cancerous tissue in less than 15 minutes.

1.2. Motivation and Novel Aspects

As discussed in the previous section, micro-scale hydrodynamic cavitation is a promising approach in treatment of some urinary tract disorders. However, so far, no suitable device is available to investigate this technique in *in vivo* surgical tests. In order to investigate the feasibility of utilizing micro-scale hydrodynamic cavitation as a new treatment modality, *in vivo* tests are necessary for exhibiting the performance of the device in treatment and assessment of possible side effects. Therefore, the major objective is to design and fabricate a biomedical device based on micro-scale hydrodynamic cavitation capable of performing an *in vivo* experiment as a novel medical intervention modality.

1.3. Thesis Objectives

This study aims to prototype a 3-D printed biomedical device, which is a flexible cystoscopy device equipped with a cavitation generating probe. Therefore, the device should be long enough to reach the bladder cavity and thin enough to penetrate to the

urethra. Also, the flexibility and steerability of the device are critical to empower the surgeon with the ability of maneuvering and locating the target zone for cavitating flow exposure.

Thus, the objectives of this thesis are as follows:

1. Design and fabricate a 3D printed long and thin steerable cystoscopy device.
2. Fabricating a long flexible cavitation probe attached to a transmission line.
3. Integrating and mounting whole parts including flexible cystoscopy probe, fluidic system, visualization system, and actuator system as a TRL6 level biomedical device.
4. Verify the effectiveness of the fabricated cavitation probe through *in vitro* tests.
5. Test the device's performance in *in vivo* tests.

2. CHAPTER TWO: MATERIALS and METHODS.

2.1. Flexible Cystoscopy Device Design

Although the prototyped cystoscopy by Abbasi *et. al.*(79) was able to locate and expose the target zone by cavitating flow in an *in vitro* environment, due to the attachment of the device to the table and short length of the prototyped device's probe (17 cm), the *in vivo* trial was not very successful to reach the desired region inside the animal body (Figure 1).

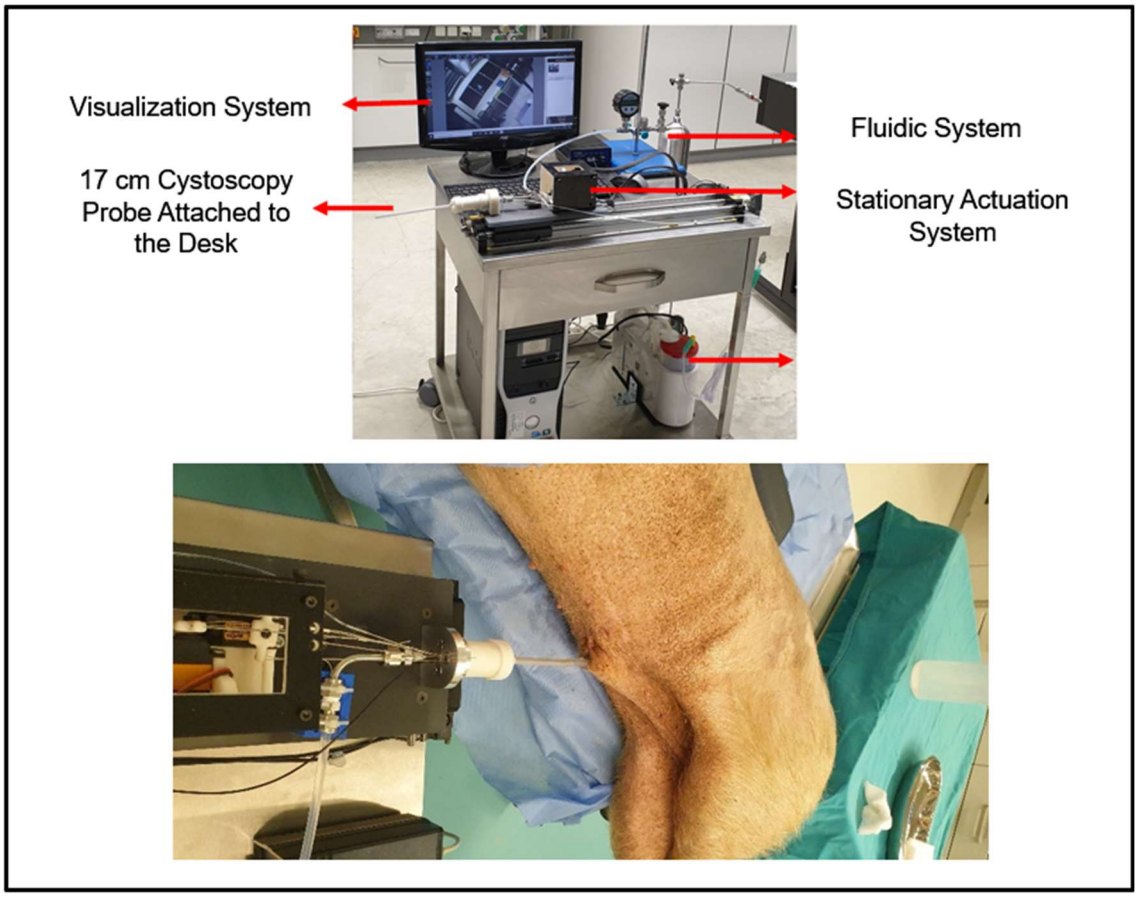

Figure 1 Previous cystoscopy prototype devised by Abbasi (80), Up) Device configuration, Bottom) *In vivo* trial.

To increase the length of the probe, a modular design based on the designs provided by Sozer *et. al.* (76) and Ghorbani *et. al.* (77) were adopted and optimized to meet the anatomical requirements of the animal's urethra by decreasing the outer diameter of the cystoscope from 10 mm to 7 mm (Figure 2). In addition to flexible segments, a guide part

with the length of 38 cm was also designed based on the capabilities of the utilized 3D printer device.

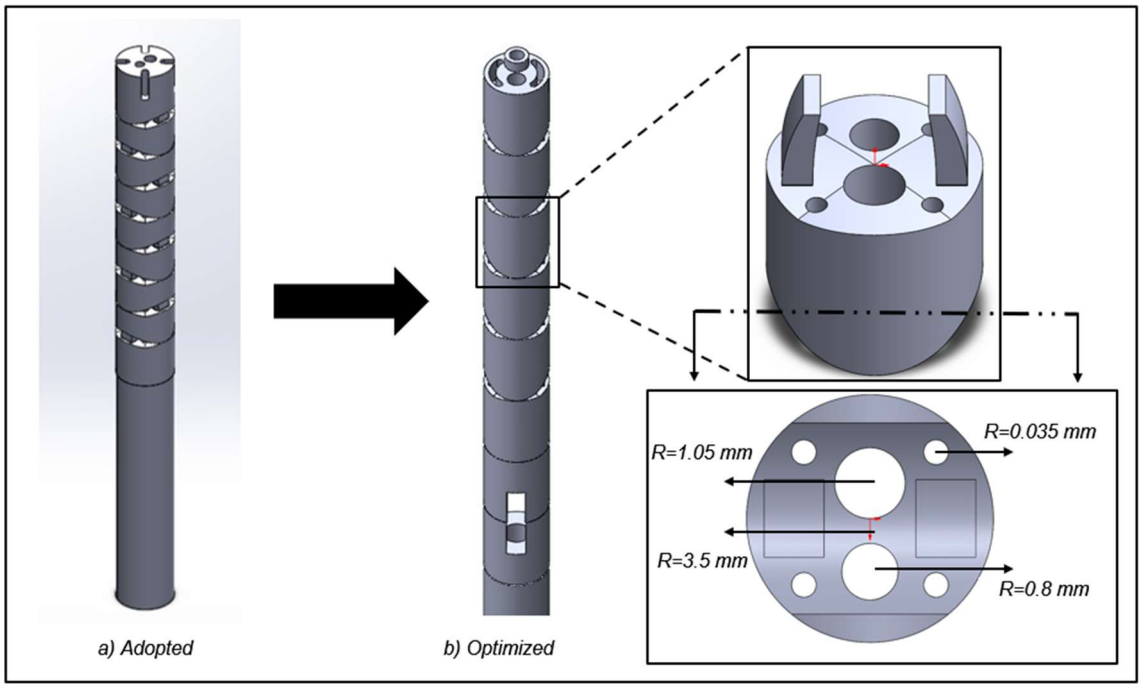

Figure 2 Optimization of the adopted probe design, a) The design provided by Ghorbani *et. al.* (77), b) Optimized design in this thesis, the upper inset is a single middle piece of flexible segments and the inset downward is the bottom cross section of the piece.

The main probe consists of 13 different separated parts categorized into four groups based on their functionality as represented in Figure 3. The flexible segments are each 1 cm long steering the medical camera and micro-scale hydrodynamic cavitation probe. The substructure segment provides the surface for the first rotation point of the flexible segments. The separating segments are used to switch the singular joint lumen in the guide part to two separated lumens of cavitation probe and medical camera. The guide part consists of two tubular outer pieces, each 19 cm long, and three 12.5 cm long inner parts (with trenches on the outer surface housing tendon drivelines) and a single 3.1 mm radius central hollow lumen. The modular design of the probe makes it possible to fabricate even larger probes without having limitations imposed by the maximum size capacity of the 3D printing device or occluded lumens.

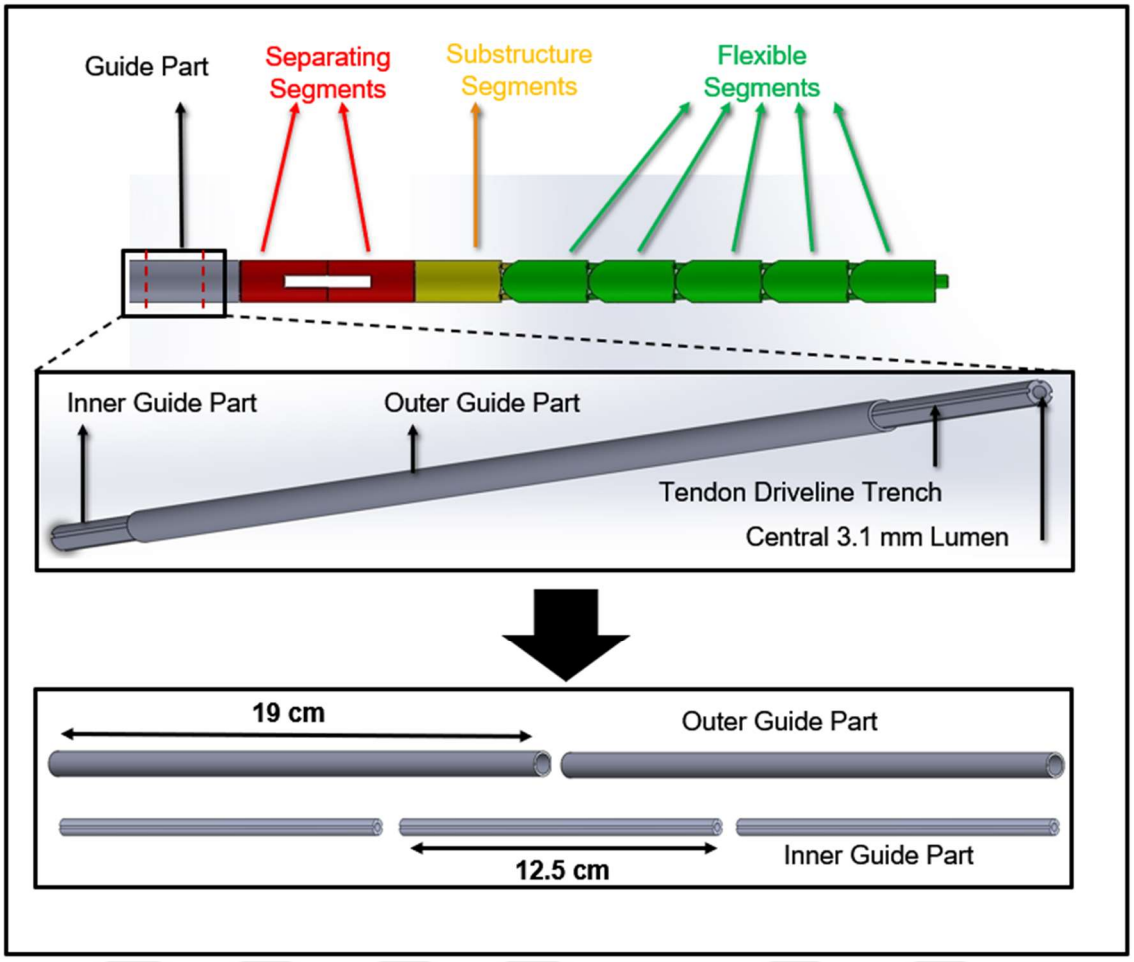

Figure 3 Schematic of different segments of the probe, Up) Total configuration, Middle) Trimmed view of the assembled guide part Bottom) Detached pieces of a full guide part.

Each flexible segment possesses especially designed surface curvatures on the top and bottom sides of the segment, which are considered the centers of rotation for the successive pieces. In addition, the bending mechanism is based on the teeth and socket joints which provides 2×8° rotation on the plane perpendicular to the axis passing through center of rotations (Figure 4). Decreasing the outer diameter of the adopted design of probe was made possible by reducing the degrees of freedom of the flexible segments part from two to one. Considering that the current design is a portable device, the operator's hand pitch restitutes the reduction of the degree of freedom.

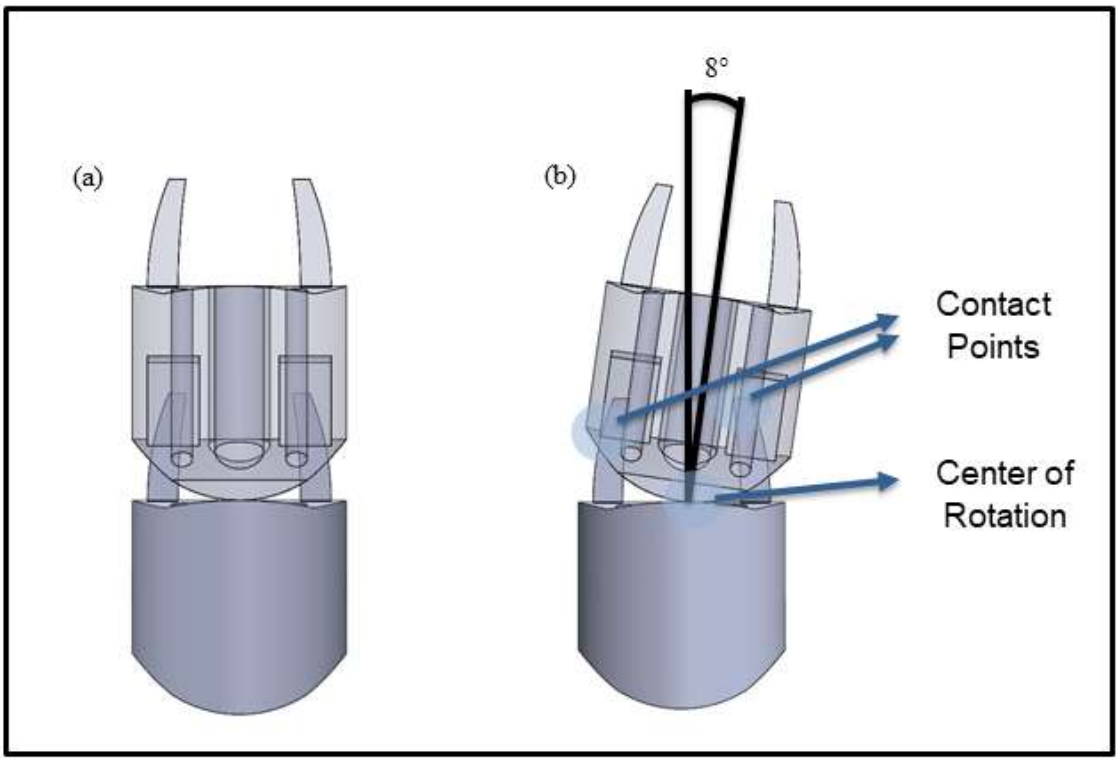

Figure 4 Bending mechanism of the flexible segments, a) neutral condition, b) maximum deflection.

Another impacting design factor in reducing the radius of the probe was implementing a mechanism, which evaded the use of stoper sleeves at the tip piece of the flexible segments. Within this design, instead of using four separate tendon lines, which anchored with a separate stopper sleeve at the tip of the probe, a U-turn hollow trench was considered, where a tendon driveline came to the tip and returned all the way back to the actuator mechanism. With this approach, the number of the separate tendon lines reduced to two, and no stopper sleeve was required (Figure 5).

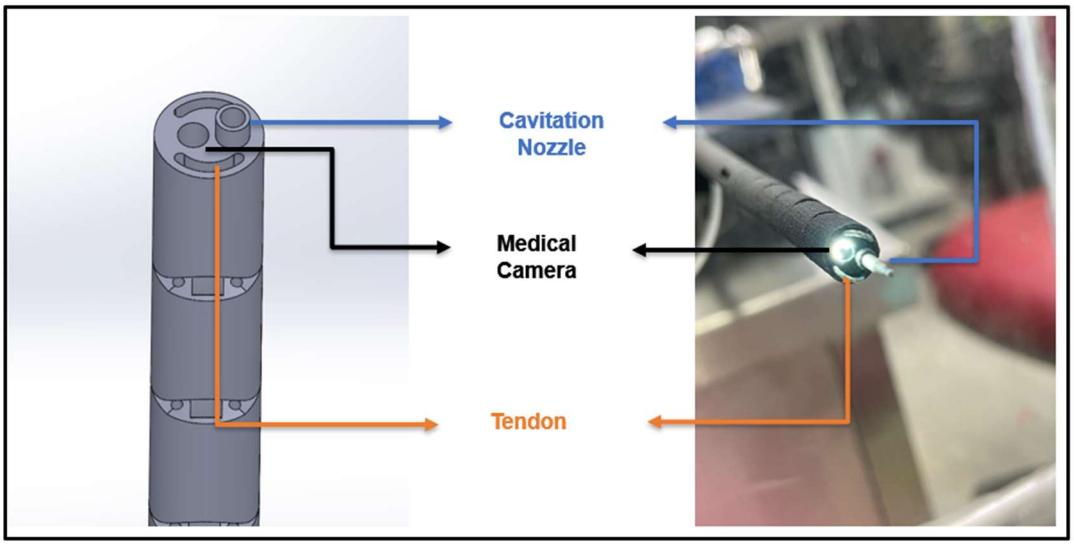

Figure 5 Tip segment design including cavitation probe place and medical camera location

2.2. Fabrication and Integration of Sub-Systems to the Flexible Cystoscopy Device

In addition to the flexible cystoscopy probe, three other sub-systems including the fluidic system, visualization system, and actuation system form the proposed biomedical device (Figure 6). In this section, fabrication and integration steps of the abovementioned sub-systems are discussed in detail. Also, an *in vitro* test setup to unravel the cavitation effect on exiting jet streams is observed.

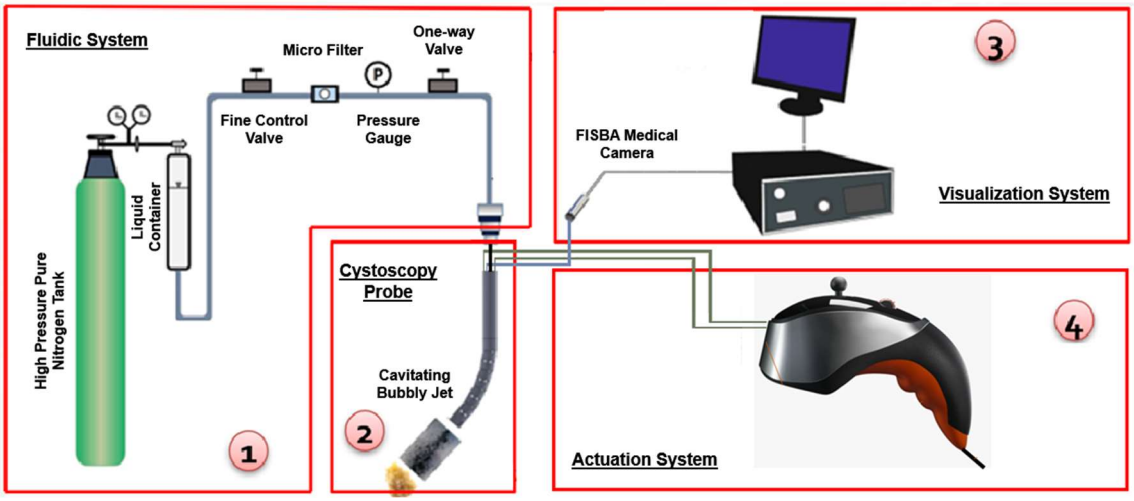

Figure 6 Schematic of the comprising sub-systems of the cystoscopy device equipped with hydrodynamic cavitation probe comprising 1) Fluidic system, 2) Cystoscopy probe, 3) Visualization system, 4) Actuation system.

2.2.1. Flexible Cystoscopy System

After designing the probe segments, 3D printed parts made of polymer would help to identify the design problems before the final fabrication step which is metal 3D printing. To fabricate the flexible cystoscopy probe's segments based on computer aided design, the first trial was performed by using the stereolithography (SLA) 3D printing device (FormLabs, Form 2). The material used for the printing was Flexible 80A Resin (FormLabs, USA). As depicted in Figure 7, the details of the segments were printed with acceptable resolution. However, the occluded tendon driveline lumens required further drilling steps, which harmed the outer wall of the segments.

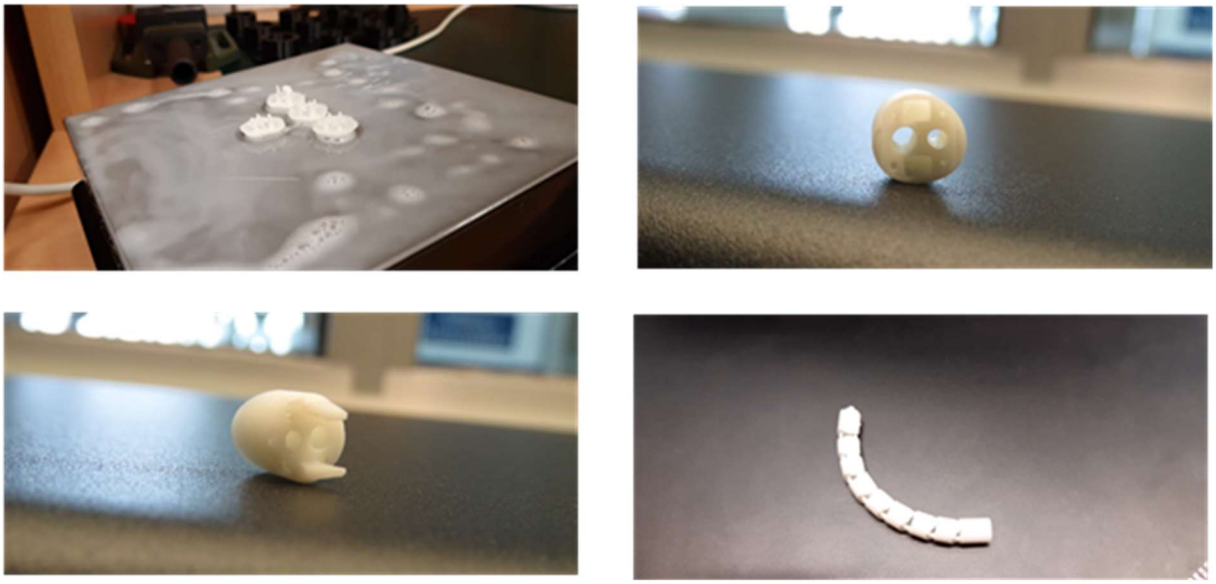

Figure 7 3D printed probe segments with SLA 3D printer

To overcome the occluded tendon driveline lumens, new parts were fabricated by the multi jet fusion (MJF) 3D printer (HP) with PA12 material. The printed pieces were all acceptable, and the tendon drive line lumens were fine. To analyze the bending performance of mounted segments, a manual joystick was also printed (Figure 8).

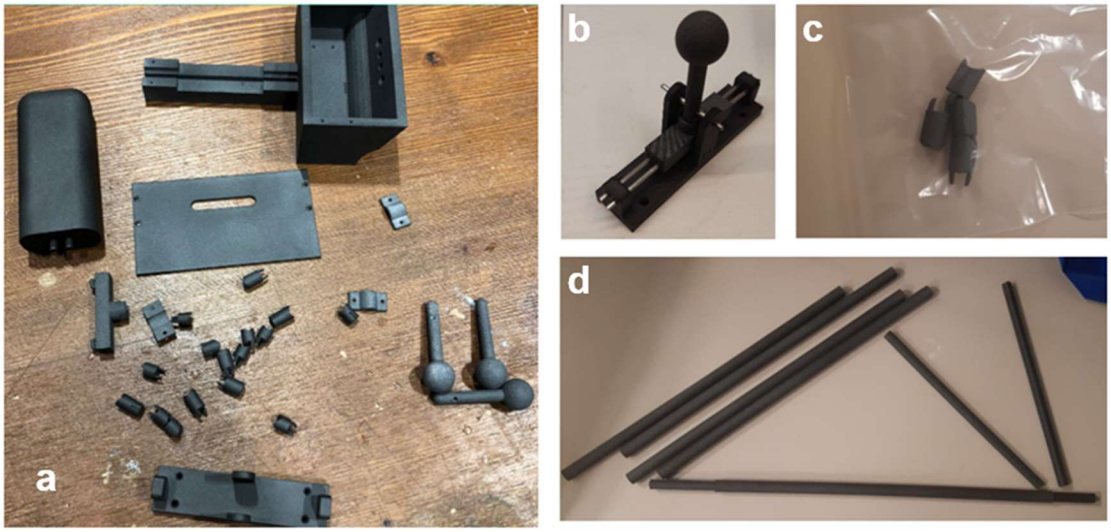

Figure 8 MJF 3D printed segments of the flexible cystoscopy device and the first version of the manual joystick, a) Joystick + flexible segments, b) Assembled inner part of the joystick, c) Flexible segments, d) Unassembled guide parts.

After revising the designs based on analyzing polymeric pieces, the metal probe was produced with two different materials including the 316L stainless steel and AlSi10Mg aluminum materials. Although production tolerances were suitable for 3D production with direct metal laser sintering (DMLS) technology, serious production problems occurred in small details for the 316L stainless steel material (Figure 9). Another issue with stain steel material was the weight of the parts.

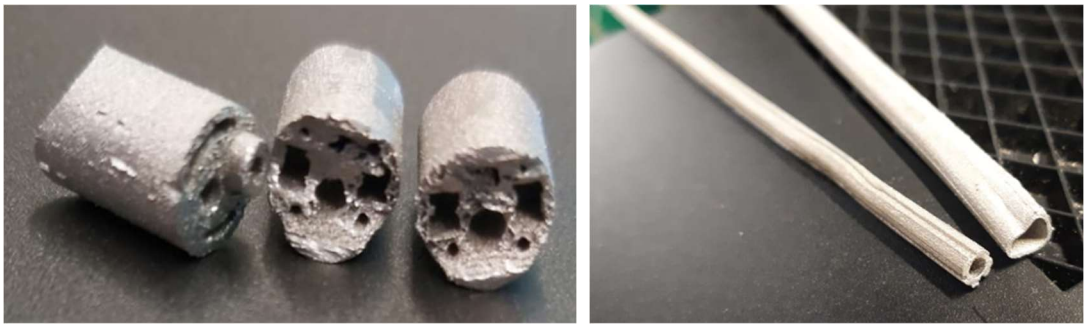

Figure 9 DMLS 3D printed parts with 316L material, the left subfigure shows the defected small segments, the right one is the defected inner and outer pieces of the guide part

To address problems with 316L material, alternative AlSi10Mg aluminum material was chosen for fabrication of the metal cystoscopy probe. The parts were defectless with higher durability compared to PA12 material (Figure10).

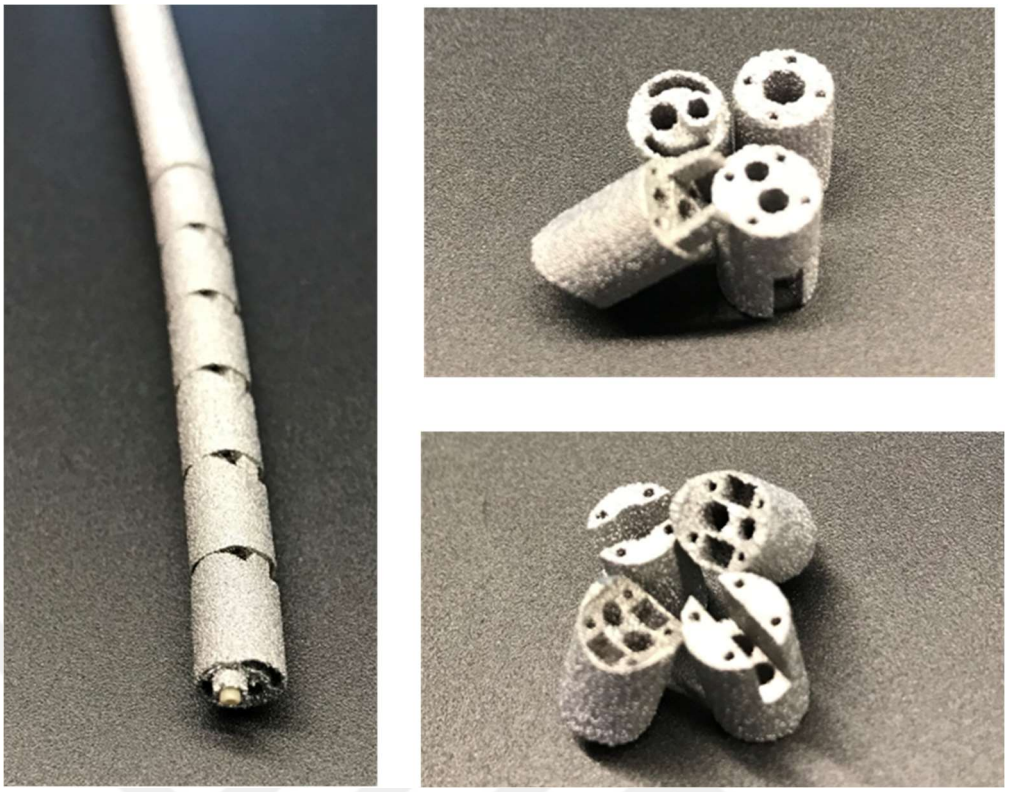

Figure 10 DMLS 3D printed parts with AlSi10Mg material, subfigure in the left shows the assembled cystoscopy probe with metal parts, subfigure in the up-right represents the top view of the small segments of the probe, subfigure in the bottom-right represents the bottom view of the small segments of the probe

2.2.2. Hydrodynamic Cavitation System and probe

The cavitation generating probe must be connected to a high-pressure fluidic system to generate the cavitating flows. The components of the fluidic system as represented in the inset number one of Figure 6 are as follows:

1. Fluid container: It is used to fill the working fluid to the system and direct it with high pressure to the pipelines. The liquid container is made of stainless steel and was purchased from Swagelok, Erbusco BS, Italy.
2. High pressure nitrogen tank: A high pressure nitrogen tank is used to provide the desired injection pressure of the working fluid.
3. Micro filter: A micro filter (Swagelok) is used to filter particles larger than 15 µm from the liquid.
4. Pressure gauges: Pressure gauges monitor the pressure of the liquid (Omega, US).

5. Control valve: Control valve (Swagelok) was installed between the cavitation probe and the fluid container to precisely control the pressure.

6. Cavitation probe: This is a 1.5-meter-long tube made of PEEK polymer with a microtube at its tip working as the cavitation generating nozzle (Figure 11).

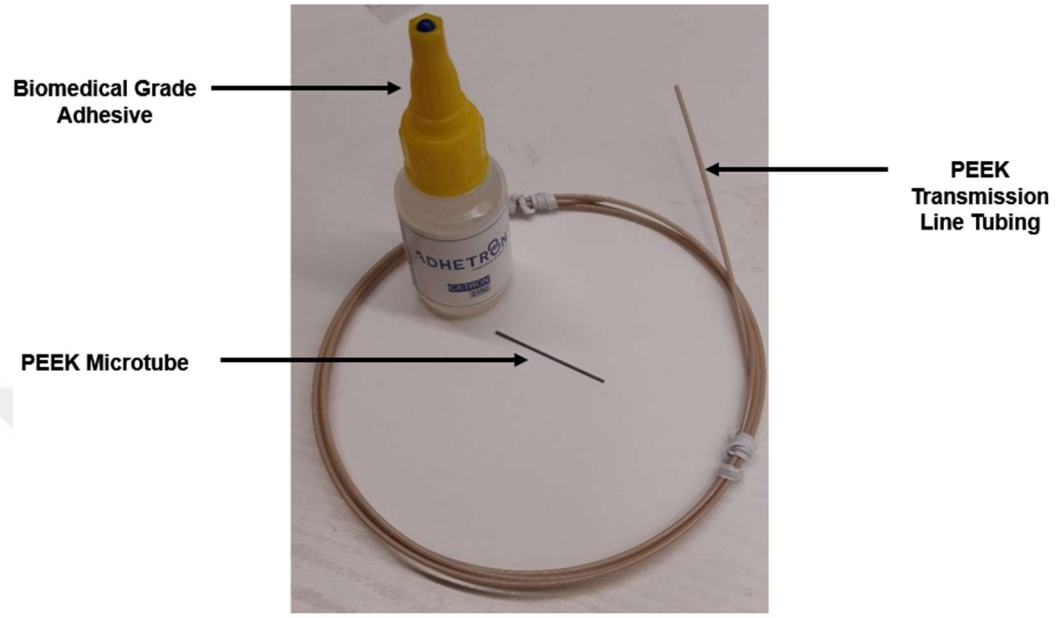

Figure 11 Cavitation probe made of a PEEK tube and a microtube attached to each other with a biomedical grade glue

The flexible cavitation probe consists of a nozzle part, a PEEK tube with different inner and outer diameters, as well as a transmission line made of a biocompatible material, polyetheretherketone (PEEK) polymer. The dimensions of the tubes used are shown in Table 1. The tubes were joined concentrically using medical grade adhesive (CA'TRON 2150). The cavitation probe has been applied to higher pressures compared to working pressure to test its durability and it has been observed that it could withstand pressures up to 450 psi (3102 kPa) under 3 hours of continuous operation.

Table 1 Cavitation probe dimensions

	Length	Outer diameter	Inner diameter
Transmission line	1500 mm	1.6 mm	1 mm
Nozzle part	10 mm	0.8 mm	0.15 & 0.25 mm

2.2.3. Driving and Control System

The used manual joystick system to control the cystoscopy probe consists of more than 20 components, where the main components can be counted as the handle, probe holder, tendon rope fixing mechanism, main case, and manual steering mechanism (Figure 12). The steering mechanism is a sliding bar which stretches the pre-stretched tendons by moving to left and right. This part was designed and fabricated at Yildiz Technical University and mounted to the flexible cystoscopy probe at Sabanci University.

Figure 12 Assembled manual joystick to the cystoscopy probe

Cystoscopy probe's segments and joystick parts were mounted to each other using two pieces of 1.5 m long silk tendon with the thickness of 0.05 mm. It was observed with the

force sensor that the total force required to bend the probe 40 degrees by pulling the right or left tendons was 50 N, and it was determined that this force was below the maximum pulling capacity of the silk tendon used (30 kg). Figure 13 represents the fully packed manual cystoscopy system.

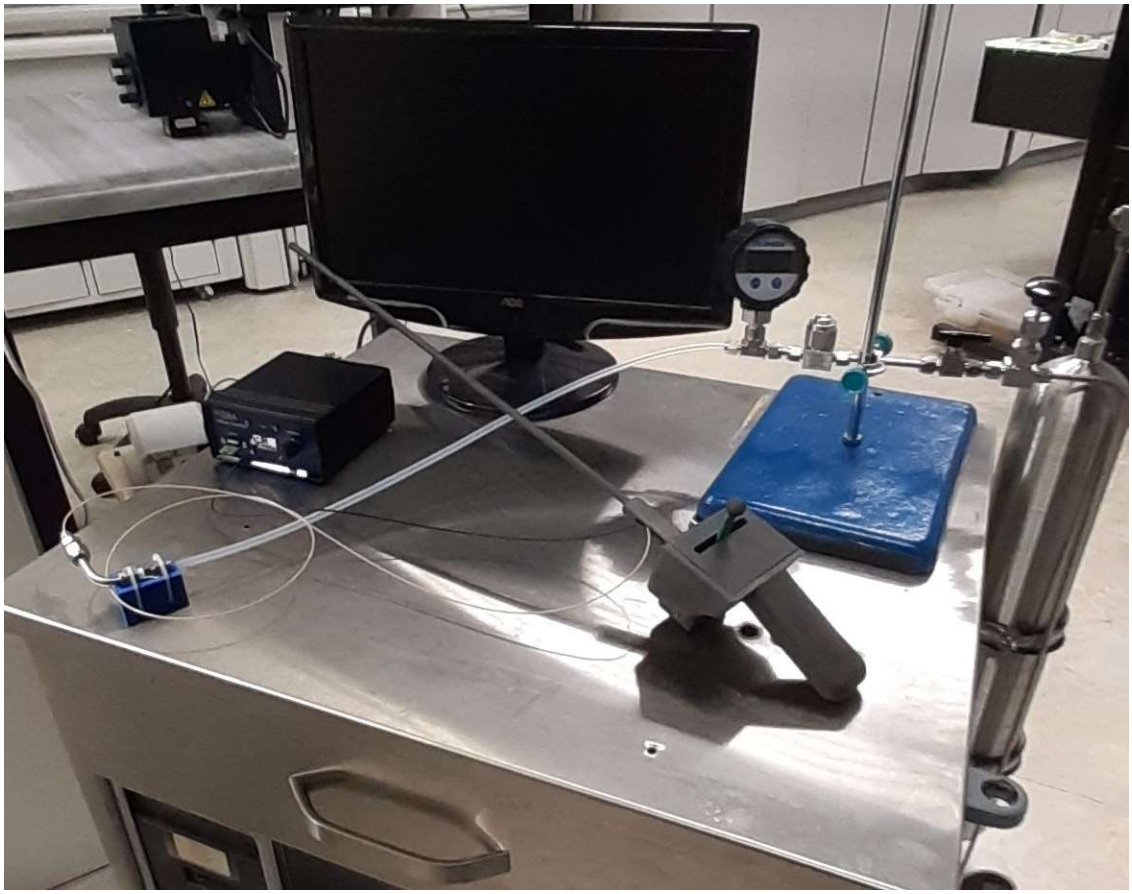

Figure 13 Fully packed manual cystoscopy system

To increase the technological readiness level (TRL) to TRL6 an automated joystick, which facilitates the handling and use of the cystoscopy device for the operator, was separately designed by the partner group at Yildiz Technical University. The utilized automatic joystick was 3D printed with MJF technology using Polyamide12 material (PA12) (Figure 14). The prototyped actuation system was mounted to the flexible cystoscopy probe utilizing a 0.6 mm thick pre-strained stainless-steel cable (Carl Stahl Sava Industries, Bare 7x19, Commercial) at Sabanci University.

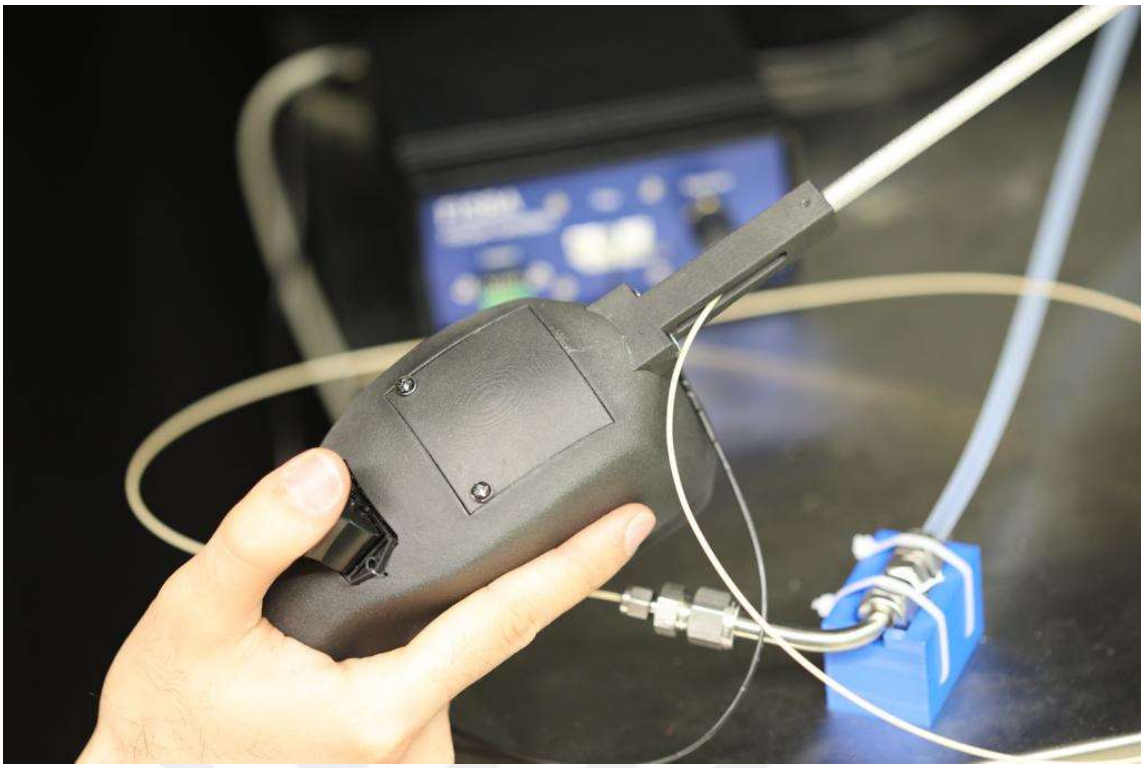

Figure 14 Assembled automatic joystick

The trials of the motor and joystick were implemented using the Savöx brand SV-1272-SG servo motor, standard Arduino finger joystick and Arduino UNO. The force transmitted by the tendons, which were attached to the servo motor head with pre-stressing, would result in rotational movement in the tip probe. The tendons attached to the servo motor head were pulled in the right or left plane with the motor movement with the command given over the joystick and within the angle range determined in the code. The angle determined in the code was adjusted in such a way that the motor advanced 1 degree in each step according to the finger joystick steering command. From its center position, the head rotated approximately 22 degrees in both directions. Due to the high output torque of the servo motor, the utilized leverage on the head of the motor was replaced with a harder plastic material, which was wear resistant.

2.2.4. Visualization System

A biomedical camera (FISCam Micro camera with illumination source) was used for the visualization of the target under the effect of the cavitating flows. The technical data of the biomedical camera is included Table 2. The lighting concept is the integrated lighting supplied by the LED and was configured through a separate control box to the glass fibers

around the camera.

Table 2 FISCam spesifications

Diameter without illumination	1.6 mm
Illuminated diameter	1.95 mm
Length without lighting	≤ 4 mm
Illuminated length	≤ 6 mm
Field of view (diagonal)	120°
Working distance	5 – 50 mm
Resolution	400 × 400 px
Bit depth	24

2.3. *In vitro* analysis of hydrodynamic cavitation in a microfluidic setup

The cavitation probe utilized in *in vivo* experiments was not transparent. To prove the occurrence of hydrodynamic cavitation phenomenon and to identify the dominant effect of cavitation implosion inside the cavitation PEEK tube, the same procedure provided in (81) was adopted by delivering a solution of 166 grams per liter KI with deionized water through the cavitation probe at three different pressures. Afterwards, the treated solution was characterized with UV-Vis, and the absorbance change was recorded. In addition, a microfluidic device with similar geometry and dimensions as the PEEK tube was fabricated according to the design and process flow provided in (82). Thus, it was possible to conduct the experiments by having the spatial control over the inception of cavitation and closely monitoring its evolution and the associated effects of bubble formation, growth, and collapse. Therefore, an experimental test rig to investigate the cavitation effect in a transparent microfluidic chip was utilized. The utilized microfluidic device contains one inlet and eight parallel micro-orifices with an open wall as the outlet, where the fluid stream exits the device. Each micro-orifice consists of lateral wall structured roughness elements. The schematic of the device is displayed in Figure 15, and the important dimensions are included in Table 3. The implemented micro fabrication techniques were included in detail in the previous study of Hosseinpour Shafaghi *et. al.* (41). Considering that the microfluidic device was tested at pressures lower than 200 psi

(lb/in²), the packaging unit of this device could easily provide visualization for inspections. A similar package was also used in the previous study of Hosseinpour Shafaghi *et. al.* (41). The patterns of cavitating flows were recorded using the Phantom VEO-710L highspeed camera. The performed visualization was based on the shadow graph technique using a light source, which illuminated the silicon surface. A K2 DistaMax macro camera lens was employed to magnify cavitating streams inside microchannels of the microfluidic device. The experimental test setup shown in Figure 15 consists of a high-pressure pure nitrogen tank (Linde Gas, Gebze, Kocaeli), a liquide container (Swagelok, Erbusco BS, Italy), stainless steel tubing (Swagelok, Erbusco BS, Italy), a pressure gauge (Omega), a T-type 2 µm filter (Swagelok, Erbusco BS, Italy), and a one-way valve (Swagelok, Erbusco BS, Italy). It should be noted that the numerical simulation of cavitating flows (79,83) inside similar tubes together with the chemical effects measurements upon bubble collapse (81) have led to the same results for the generation of desired cavitating flow patterns. As the final step, *in vitro* tissue experiments were carried out exposing the porcine bladder and urethra tissue to cavitating flows with the use of the cavitation probe for 5, 10, and 15 minutes in the laboratory environment with the same procedure done by (80), and pathological analysis of tissues and cells were performed accordingly.

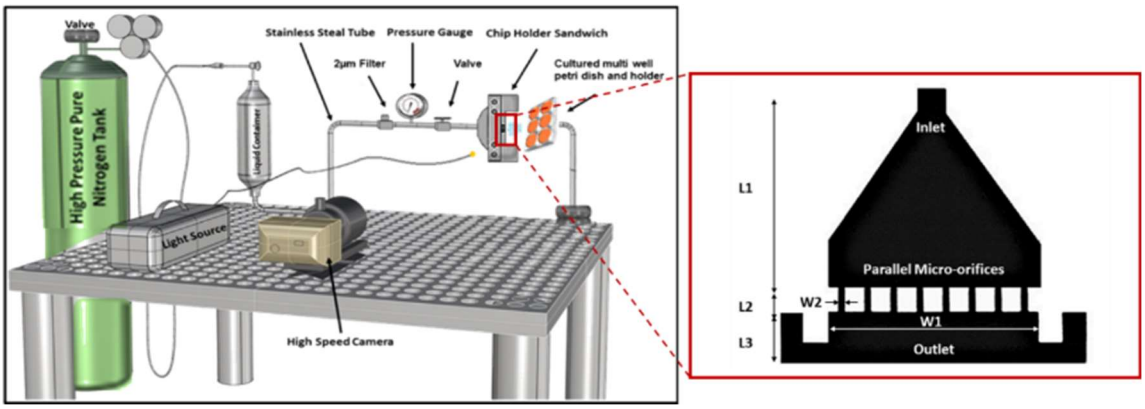

Figure 15 Schematic representation of the test setup consists of a high-pressure pure nitrogen tank, a liquid container, stainless steel tubing, a pressure gauge, a T-type 2 µm, and a one-way valve.

Table 3 Important dimensions of the Microfluidic chip

Displayed at the inset of Fig. 16	L1	W1	L2	W2	L3	Roughness Height	Roughness Length	Channel depth
values are in (μm)	2000	7800	1000	300	2000	3	1000	50

3. CHAPTER THREE: RESULTS and DISCUSSION

3.1. Device Performance

3.1.1. Cystoscopy probe and cavitation probe

The mounted flexible cystoscopy probe contains 5 pieces of flexible segments, which implies that it is able to bend 40 degrees to each side of the neutral position of the probe on the perpendicular plane to the rotation axis. As shown in Figure 16, the probe can bend 39 degrees.

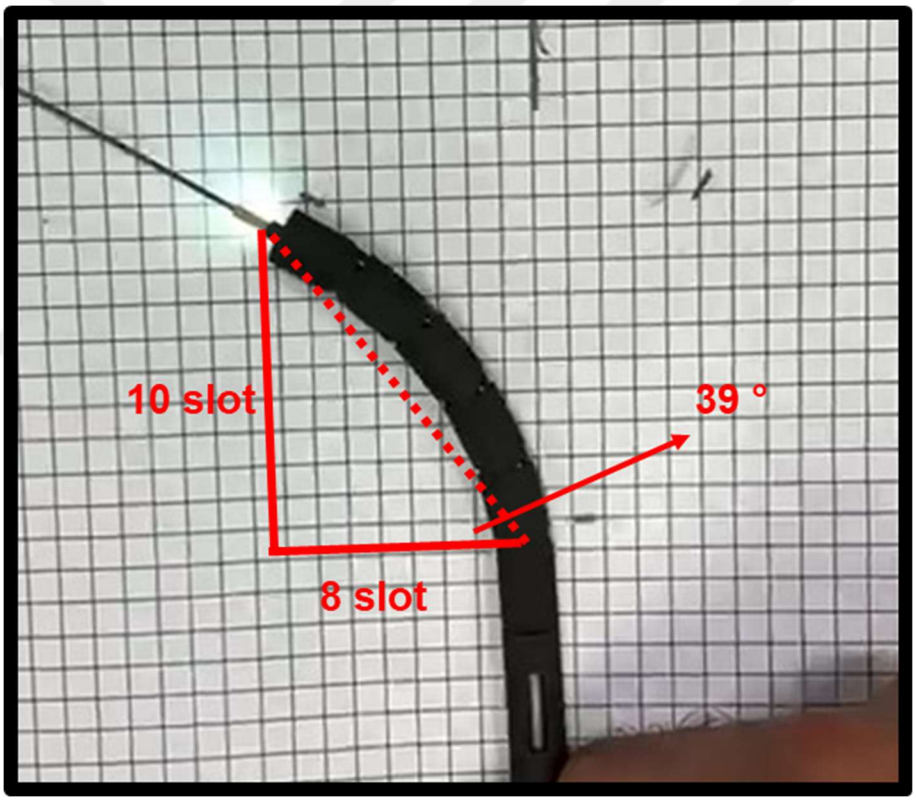

Figure 16 Bending performance of the flexible cystoscopy probe

The total length of the prototyped cystoscopy probe as one of the objectives of this thesis was successfully increased to 46 cm (with the thickness of 7 mm), which is acceptable for penetrating through the urinary tract (Figure 17).

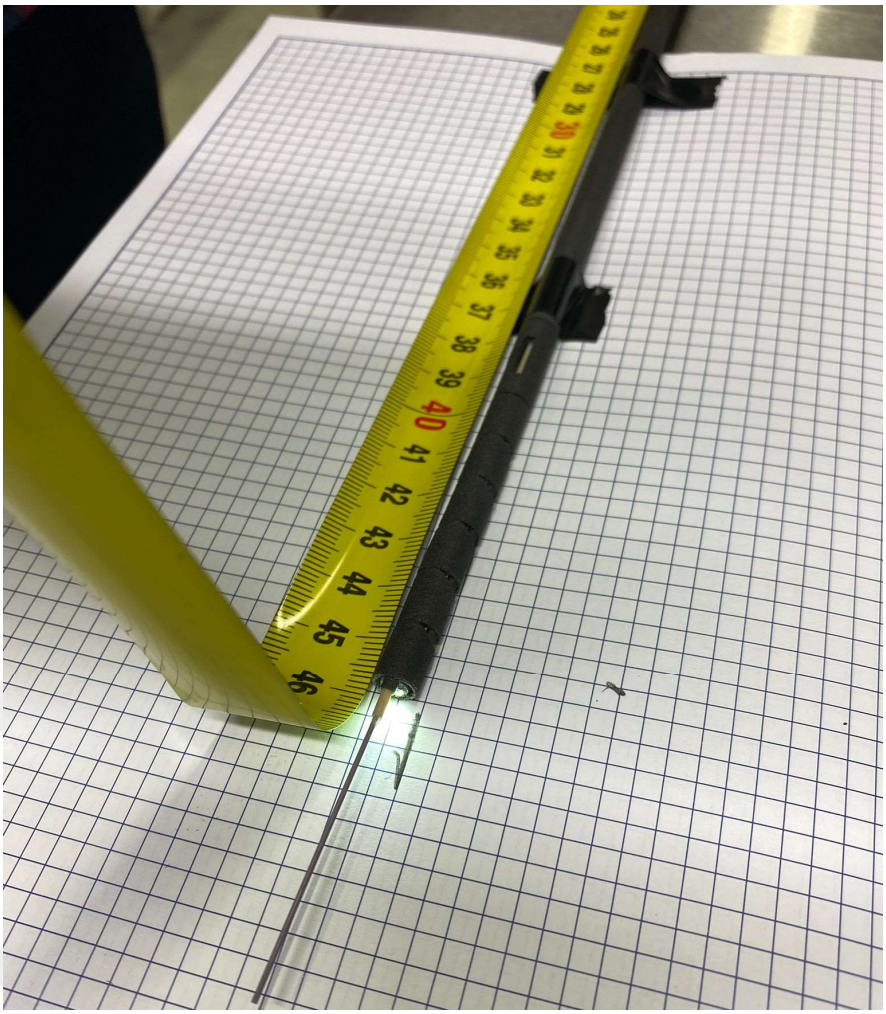

Figure 17 Length of the prototyped cystoscopy probe

3.1.2. Cavitation probe

Fabricating a flexible long cavitation generating probe was vital to prototype the hydrodynamic based cystoscopy device. As represented below (Figure 18), cavitation generating nozzle technologies comprise three generations. Koşar *et. al.* (71) designed the first generation, where a microtube was integrated with rigid stainless tubing. Abbasi *et. al.* (79) used a semi flexible chromatography stainless steel tubing for their proposed device. However, the probe was not long and flexible enough to be used in the fabricated flexible cystoscopy probe. Therefore, the fabricated cavitation probe in this thesis was made of PEEK tubes with two different sizes proposing novelty and very efficient method regarding the use of hydrodynamic cavitation in biomedical research efforts in *in vivo* tests.

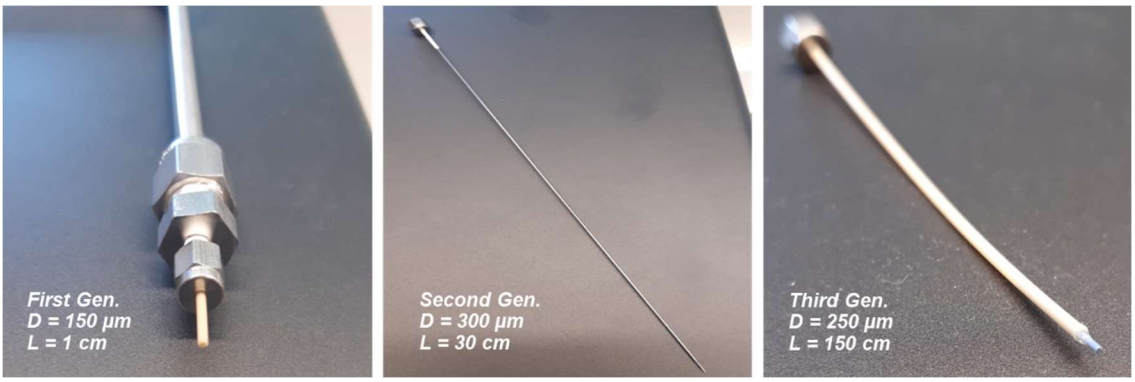

Figure 18 Right) First generation cavitation jet probe, Middle) Second generation cavitation probe, Left) Third generation cavitation probe.

Verifying the cavitation flow regime inside the prototyped cavitation nozzle was caried out by the proposed method in reference (81) by using a concentration of 166 gram/liter KI solution with deionized water, where the hydrodynamic cavitation flow patterns affect the I^- oxidation in a different manner in response to chemical or mechanical effects of the cavitation collapse. Figure 19 shows the UV-Vis results of the KI solution exposed to cavitation pertinent to different inlet pressures.

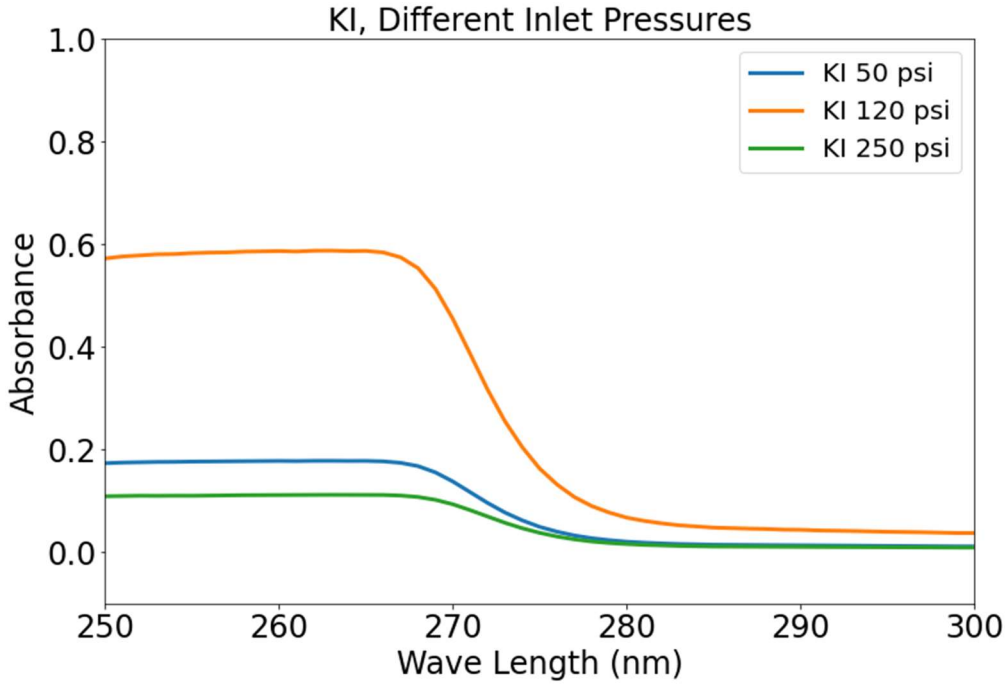

Figure 19 UV-Vis results of KI test indicate that cavitation incepts at 120 psi, and the intensity increases with the pressure to 250 psi, where no chemical effect was observed

As discussed in the mentioned reference (81), chemical effects are dominant at pressures close to cavitation inception, and mechanical effects play an important role in fully developed flow. In other words, UV-Vis characterization results in Figure 19 manifests that the cavitation nozzle experiences cavitation inception at 120 psi. Upon an increase in the pressure up to 250 psi, as the absorbance decreases, cavitation flow regime makes transition to choked cavitation pattern.

3.1.3. Finalized assembled cystoscopy device

The finalized assembled compact version of the flexible cystoscopy device with automatic joystick, consisting of a flexible metal 3D-printed probe, automatic joystick, stainless steel tendon cables, medical camera system, cavitation probe and high-pressure fluid line system is shown in Figure 20.

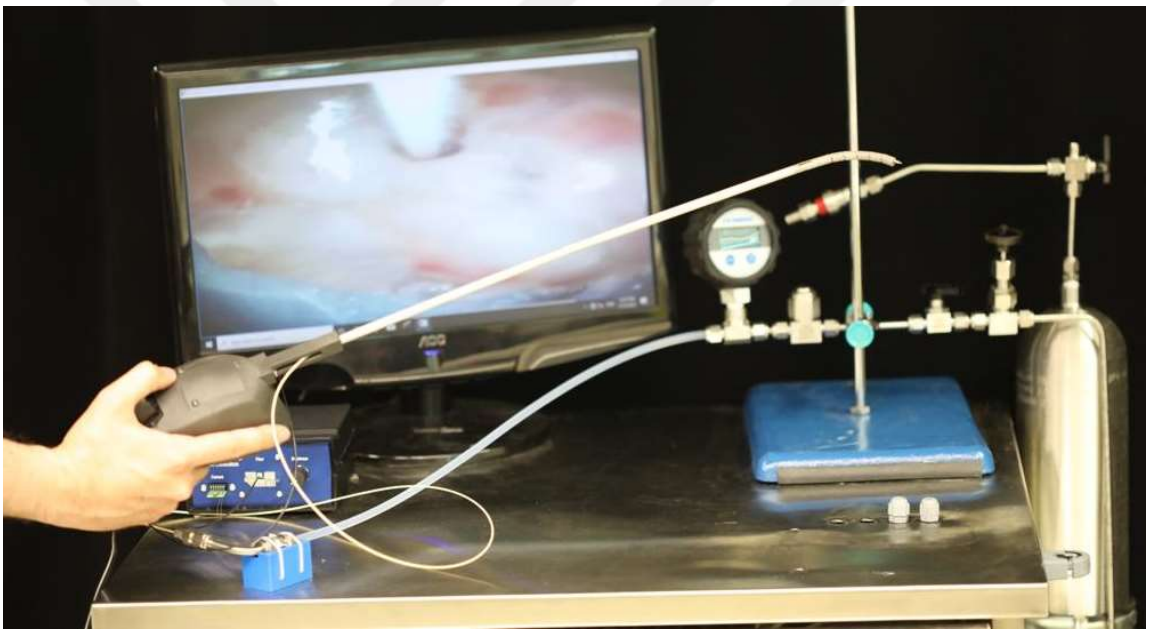

Figure 20 Flexible cystoscopy device with an automatic joystick

3.2. *In vitro* results

3.2.1. Cavitating flow patterns visualization

Within the fabricated microfluidic chip, cavitation occurs at both the Vena Contracta region of the inlet of each micro-orifice, and the exit region of each micro-orifice at the

outlet. The formation and evolution of cavitation at the outlet of each micro-orifice is important because it affects the direction and characteristics of jet streams exiting from parallel micro-orifices. Moreover, due to cavitation bubble collapse, atomized droplets are generated and carried together with the fluid and the vapor stream (Figure 21) bombarding samples placed in front of jet streams with cavitating flows. This effect happens in a cyclic manner with a lifespan of sub milliseconds for each cycle. The size of the atomized droplets that are produced as a result of the hydrodynamic cavitation can range from sub-micron to several microns and impinge on the cell membrane of the target. At the outlet region, as shown in figure 3, exiting streams from each of the micro-orifices carry a twin vapor sheet jet surrounding the fluid flow, and due to the presence of hydrodynamic instabilities such as Kelvin-Helmholtz instability (84), cavitation cloud shedding occurs initiated by semi recurring collapses of attached cavities around the stream. In addition, in the outlet region as a consequence of vortex formation, which was also previously reported (82), some streams converge and merge with each other and eject the microfluidic device as a converged jet (Figure 21).

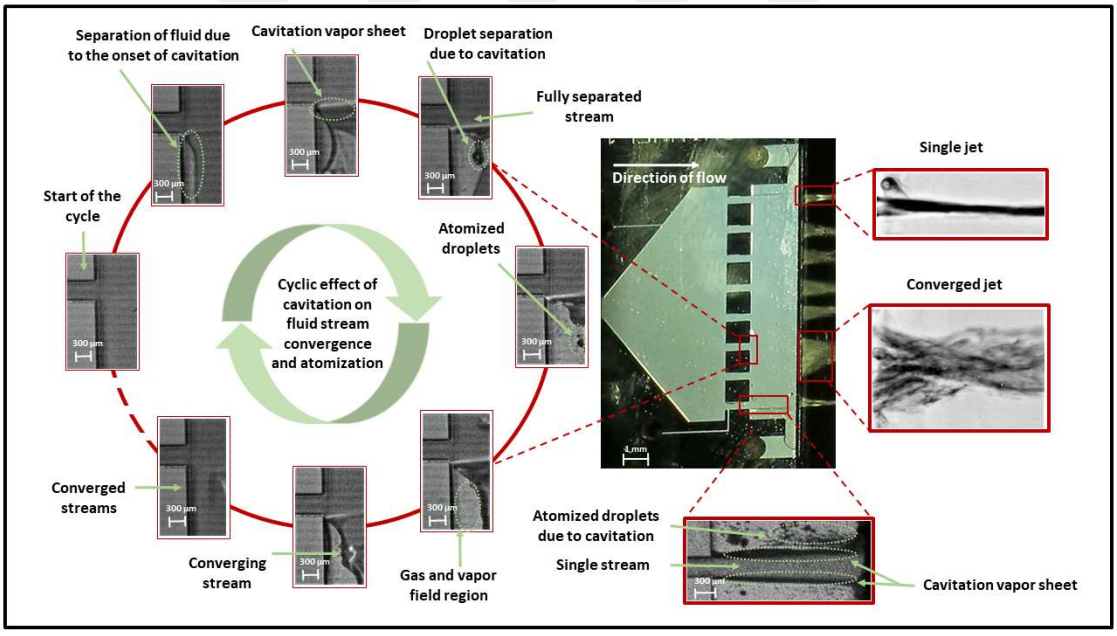

Figure 21 Visualization under the effect of cavitation within the microfluidic chip (middle). On the left side, the cyclic effect of cavitation on droplet atomization and jet stream convergence are displayed. On the right side, two different types of single and converged jet streams are visualized using shadow graph technique. At the bottom, the presence and spatial location of atomization and vapor sheet on each single stream is shown.

3.2.2. *In vitro* cell and tissue results

SEM images of immobilized cells exposed to hydrodynamic cavitation by the microfluidic device reveal membrane poration sites with micron and sub-micron size scale, which represents the effect of cavitation bubbles and atomized droplets impinged to the cell membrane. Cell lines exposed to hydrodynamic cavitation were HCT-116, Beas-2b, and SHSY-5Y (Figure 22).

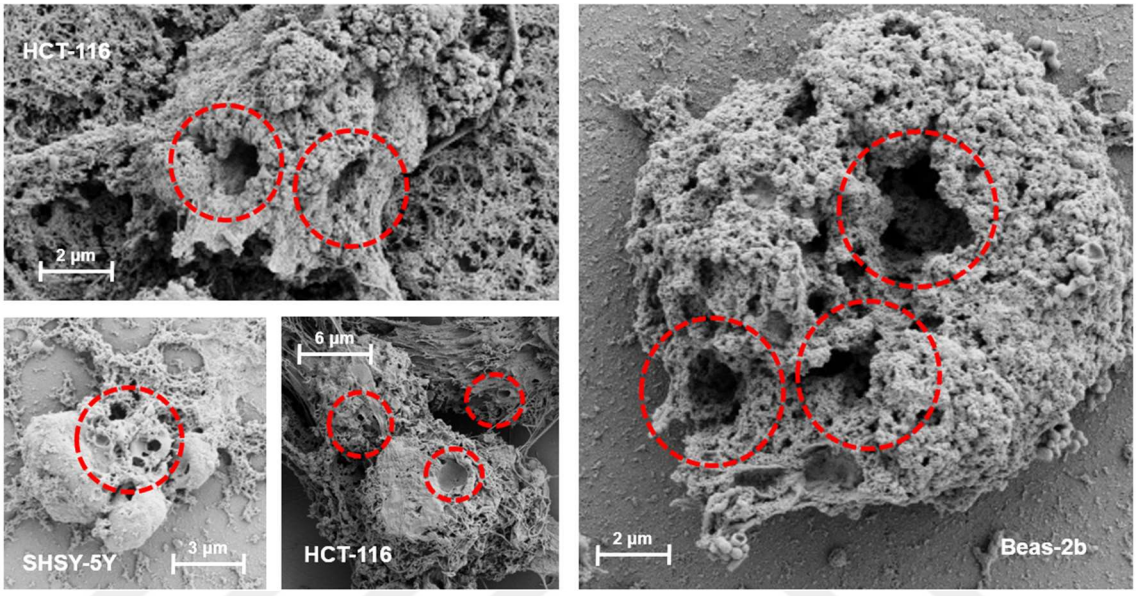

Figure 22 SEM images of immobilized cells exposed to hydrodynamic cavitation

Pathological analysis on the cavitation effects on porcine bladder and, urethra tissues and cells are represented in Figure 23. Upon the application of cavitation at 150 psi for 5 minutes, 10 minutes and 15 minutes, cavitation caused tissue losses in the target area, and signs of death such as disruption of the cell nucleus structure in the cavitation border line were observed. Also, it was shown that no harmful effects occurred in the area except the target (Figure 23).

The evaluation of the cavitation exposed area reveals approximately 0.5-0.6 mm ablation in bladder and urethra tissues. This value is clinically comparable to the 0.8mm ablation effect of the 80W KTP (potassium-titanyl-phosphate) 512 nm laser on the prostate tissue (85), which has thinner muscle tissue compared to bladder and urethra. On the other hand, no tissue loss or cell death was observed in the control samples with the jet flow rate of the main probe for the no cavitation case. According to a previous study (73) conducted with BPH tissue, an effect of approximately 0.16 mm was observed in the control samples

within 15 minutes, while this depth was increased to approximately 0.48 mm in the treated samples with the new cavitation probe.

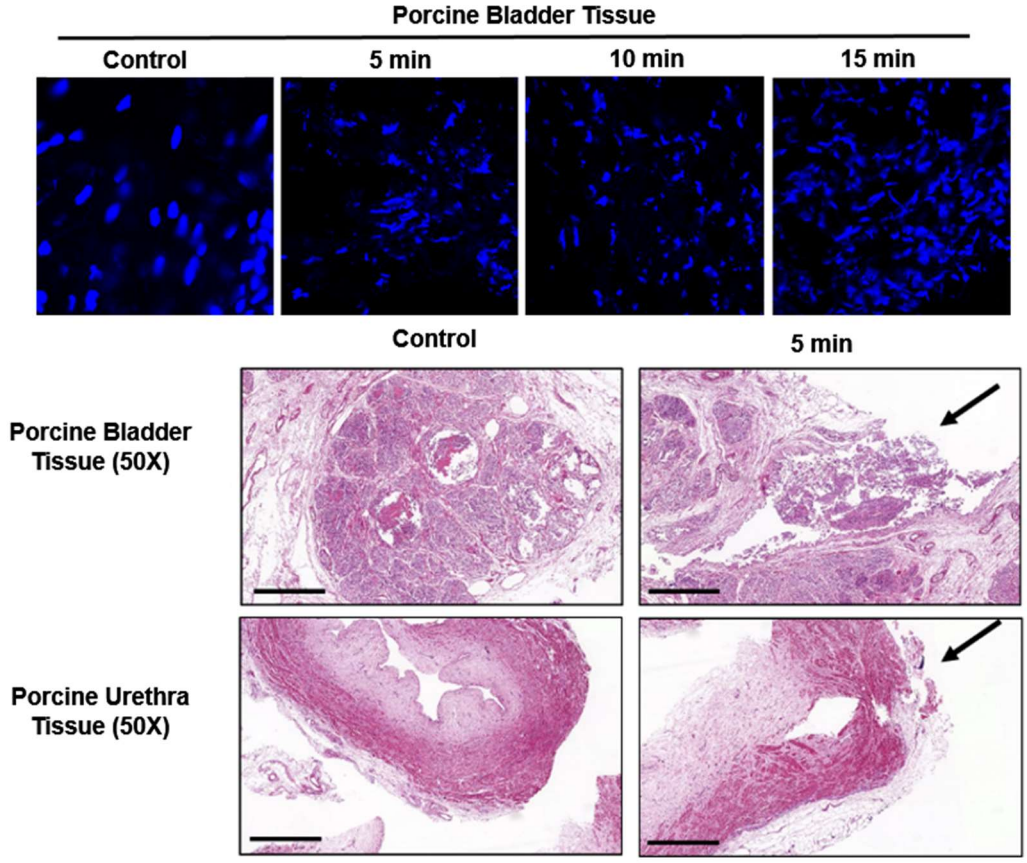

Figure 23 Up) Time-dependent variation of the effect of cavitation on cellular structure in porcine bladder tissue. Blue color indicates cell nuclei stained with DAPI. Bottom) Pathological analysis by H&E staining of porcine tissues exposed to cavitation for 5 minutes with the no-cavitation control. Scale bar indicates 62.5μm at 50x magnification. Black arrow indicates cavitation angle.

3.3. *In vivo* results

After finalizing the cystoscopy device and having the approval of the ethics committee, *in vivo* tests were conducted by the urogenital surgeon, Prof. Dr. Sinan Ekici, at the Acibadem University Hospital. The medical intervention was performed on a female porcine (Figure 24). The probe was successfully penetrated inside the urethra. Real-time visualization of the tip of the probe allowed the surgeon to move along the urethra using the automatic joystick. Water was continuously supplied from the cavitation probe at

pressures lower than the cavitation inception to ensure sufficient fluid within the urinary tract for visualization purposes. After determining a target region in the urinary tract, the probe approached and aimed the target (Figure 25). The fluid pressure was increased to 200 psi, where cavitation occurred and was exposed to the target for the duration of 20 minutes.

Figure 24 *In vivo* trial of the prototyped cystoscopy device

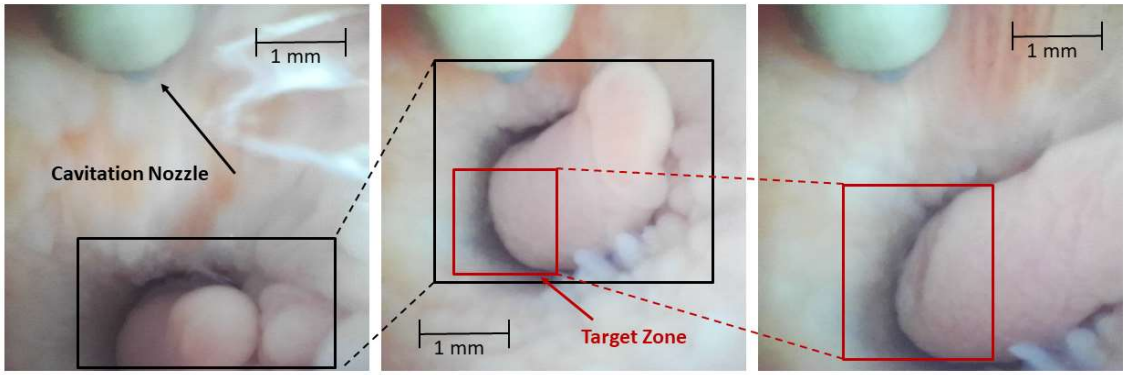

Figure 25 Visualization of the cavitation probe approaching to target while working inside the urinary tract

After the process was complete, the exposed tissue was extracted and sent for pathology

analysis. According to histopathological results, at the zone where cavitation was applied, an area of melting was observed with clear borders in the mucosa. The formation of a cavitary area was observed macroscopically. In the microscopic examination of the sections prepared from paraffin blocks of the tissue representing this area (Olympus BX-51), an area of melting and tissue loss was observed with clear borders in the mucosa and submucosa. Vascular structures and interstitial tissues were observed in normal appearance. Hematoxylin and Eosin-stained preparations were scanned in the Virasoft digital microscopy scanner and digital microscopic images of control tissues and tissues that were exposed hydrodynamic cavitation were recorded (Figure 26).

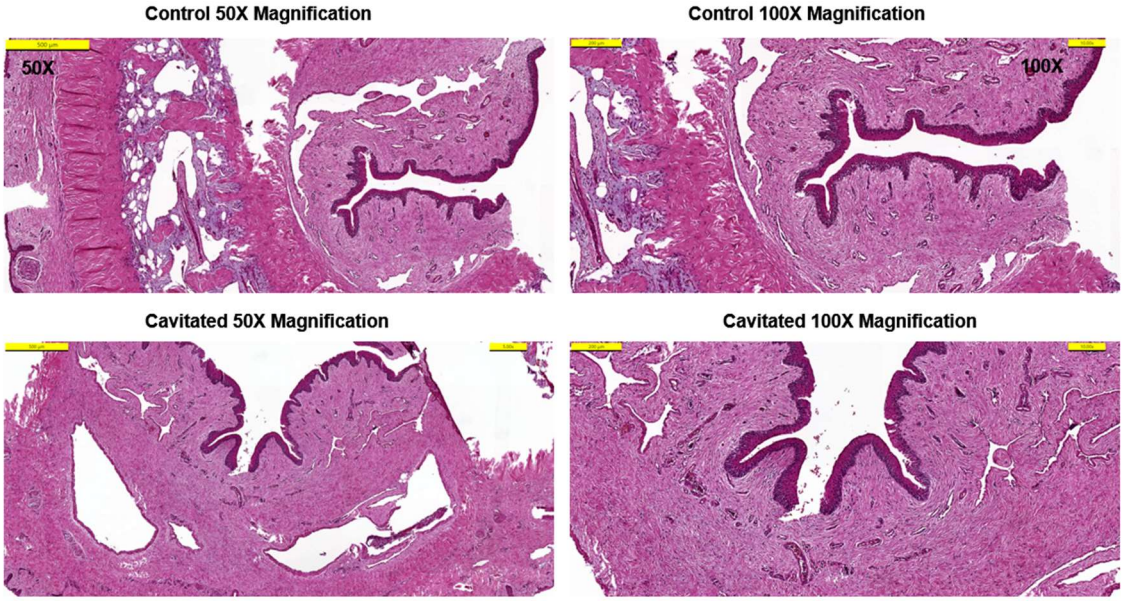

Figure 26 Pathological analysis by H&E staining of porcine tissues, Up) Control sample (no exposure to cavitation), Bottom) *In vivo* samples exposed to cavitation for 20 minutes with 200 psi upstream pressure

4. CHAPTER FOUR: CONCLUSION

4.1. Flexible Cystoscopy Device based on hydrodynamic cavitation

A metal 3D printed flexible cystoscopy probe equipped with hydrodynamic cavitation jet nozzle was successfully tested on a porcine *in vivo* test and the results showed the efficiency of the approach in ablation of ill tissues tests. Therefore, the proposed device, which is economically superior to laser based or acoustic based methods, provides a comparable final output in ablation of soft tissues. Table 4 represents the price of the parts used for prototyping the current device. Based on the given pathology results, a sharply demarcated tissue defect occurred in the epithelial and subepithelial tissue in the area of cavitation exposure. In addition, there was no obvious tissue or cell damage in the area around the defect.

Table 4 Price of the utilized parts to prototype the device

	Price in USD
Visualization System	6500 $
3D Printed Parts	250 $
Actuation System	250 $
Cavitation Probe	100 $
Fluidic System	1800 $

To ensure that the cavitation happens within the fabricated cavitation probe, separate tests using KI solutions were carried out. Accordingly, cavitation inception occurs at a pressure near to 120 psi, and the mechanical effect of cavitation collapse becomes more dominant upon the pressure increase. To better understand the effect of cavitation on flow patterns of the exiting jet, a parallel experiment using a microfluidic chip with similar critical dimensions to the fabricated cavitation probe was scrutinized, where micron sized atomized droplets were generated due to the cavitation cloud collapse near the liquid stream. Also, cavitation effect on the cell membrane poration was analyzed by bombarding immobilized cells with the cavitating flows inside the microfluidic chip. SEM images of bombarded cells revealed micron sized pores on the surface of cell membranes. *In vitro* porcine tissue ablation experiments were conducted to probe the

effectiveness of hydrodynamic cavitation through pathology analysis. As the final step, *in vitro* tests with the developed 3D printed cystoscopy device was performed. The previous shortcomings stemming from the short length of the probe and attachment of the device to the desk were eliminated by the proposed design and prototype. Two different materials (PA12 and AlSi10Mg) were used to fabricate the final probe, which allowed a light portable device. During the *in vivo* tests, it was observed that the servo motor used for the automatic joystick was over-heating, which could be evaded by using a smaller servo motor with lower output power. Considering the outstanding performance of the developed cavitation probe, it could be contemplated that the probe has a huge potential to be used in other industrial or bio related applications such as thrombolysis.

4.2. Future Research Direction

Although recent developments in the field of micro-scale cavitation proved its wide applicability and opened new research lanes in various fields, there is still room for improvement in potential of cavitation-on-a-chip devices and understanding of physics of micro-scale cavitation in mechanical, thermal, and chemical aspects as the main effects of the bubble collapse. While cavitation in macro-scale is a well-established field, most of the studies have been executed in laboratory scale, which implies that the limits should be pushed to extend these outcomes to industrial scale. This challenge in conventional scale studies should be a model for micro-scale investigations to tackle global valuable issues related to energy and healthcare.

When it comes to the collapse of bubbles, there is still a lack of adequate information about bubble rupture. Also, these developments should address the chemical effects of bubble collapse. The fundamentals of the thermal behavior in nonlinear bubble dynamics and its relationship with chemical outcomes were parametrically investigated by some researchers (86). However, the pyrolysis mechanism of the contaminant and pollutants and impingement of radicals of species to the target for the degradation have not been well understood.

Compared to macro-scale studies, the potential of tracking the successive impacts of bubble rupture is very promising due to extremely finite domains. Moreover, in-depth analysis involving the bubble shape (spherical and non-spherical), multiple phenomena and scale effects is required to realize its implementation in the industrial applications

(87).

Developing the theory of the bubble generation and collapse and understanding its physics will lead to utilization of the collapse effects in different applications. Micro-scale cavitation could be used in wastewater treatment, oil refinery, cleanings, energy harvesting and nanomaterials production. The key element here is understanding mechanical and chemical behavior of bubble collapse in both individual and in combined manner. Micro-scale cavitation could propose a precise platform, which could assist researchers in focusing energy released from the bubble collapse to small spots. The local erosion due to mechanical effects of the bubble rupture could be investigated in more detail in micro-scale thanks to rapid developments in nanotechnology and surface engineering.

Considering the need for utilizing an ecologically friendly advanced oxidation process as an alternative to chemical-induced methods, it is expected the micro-scale cavitation could introduce a global solution for the degradation of micro-organisms in in both micro and nano scales in disinfection and tertiary steps of wastewater treatment plants. It is predicted that the micro-organisms, organic and non-organic materials such as active pharmaceutical ingredients, gram-negative bacteria, viruses, cyanobacteria microalgae will be the potential targets for the use of the collapse energy of cavitation bubbles (10,88). It should be noted that micro-scale cavitation could be used solely or in combination with other advanced oxidation processes i.e., UV and ozonation to achieve an optimum degradation rate.

Despite many shortcomings and uncertainties in the literature and industry, the energy stored in cavitation bubbles offer great potential to be elucidated and used in bio-related applications. Cell engineering, where cavitation in micro-scale could be a promising approach to permeabilize the cell membrane, has attracted the attention of some researchers during recent years(89,90). For successful implementation, a full control over the bubble generation, dynamics and implosion is needed to permeabilize the cells consistently without excessively lysing them (91). In addition, studying cell response to mechanical stimuli (mechanotransduction) of bubbles is important and requires devising smart experimental approaches (to give an insight, readers are invited to check Chen *et. al.* (92)). Therefore, cavitation-on-a-chip devices could serve for offering controlled localized energy release and probing cell response. In this regard, Li *et. al.* (93,94) investigated the cavitation-induced calcium response of HeLa cells using a microfluidic

chip equipped with laser induced tandem bubble generating system to study the bioeffects of bubble-cell interaction. They claimed that their technique was reliable and reproducible with the limitation of having a single-use device. Alongside with reliability and consistency, a high throughput device for intracellular delivery is of great importance (95). Hydrodynamic cavitation-on-a-chip device could be a solution because of its inherent high flowrates. Developing such microfluidic chips requires a profound insight on mechanical, thermal and chemical bioeffects of micro-scale cavitation on cells, which suggests the need for more in-depth investigations.

Another possible lane for micro-scale cavitation is the use of destructive energy of collapse for ablating or lysing unwanted tissues or entities inside the human body. For example, high intensity focused ultrasound (HIFU) and lithotripsy, both associated with the activation of cavitation nuclei inside tissues and surrounding liquids, has long been known and used for kidney and gal stone fragmentation (interested readers are invited to refer to Bailey *et. al.* (96) as well Ghorbani *et. al.* (97)). As another instance, ultrasound assisted thrombolysis was introduced as an alternative treatment method for patients with acute pulmonary embolism complications(98). It was shown that cavitation mechanically damaged the clot during sonothrombolysis (99). Catheter-delivered transducer-tipped ultrasound devices have led to promising results when used in combination with thrombolytic agents or together with microbubbles (100,101). It was also reported that the success rate of new mechanical thrombectomy devices (not associated with cavitation) without conjunction with thrombolysis agents was 50% (102). On the other hand, studies on biomedical applications of hydrodynamic cavitation revealed the capability of cavitation to ablate the undesired entities inside the body (103–105). Therefore, hydrodynamic cavitation appears as a practical method of thrombolysis, which could refrain the use of thrombolytic agents. The most important obstacle in the use of hydrodynamic cavitation method is the high amount of ejected fluid, which requires evacuation. Thus, utilization of this concept in organ-on-a-chip studies could pave the way to novel solutions in bio-related applications.

REFERENCES

1. Brennen CE, Oxford NY. Cavitation and Bubble Dynamics. 1995;
2. Young FR. Cavitation. World Scientific; 1999.
3. Suslick KS, Flannigan DJ. Inside a Collapsing Bubble: Sonoluminescence and the Conditions During Cavitation. Annual Review of Physical Chemistry. 2008 May 1;59(1):659–83.
4. Flannigan DJ, Suslick KS. Plasma formation and temperature measurement during single-bubble cavitation. Nature. 2005 Mar;434(7029):52–5.
5. Sinibaldi G, Occhicone A, Alves Pereira F, Caprini D, Marino L, Michelotti F, et al. Laser induced cavitation: Plasma generation and breakdown shockwave. Physics of Fluids. 2019 Oct 1;31(10):103302.
6. Didenko YT, Suslick KS. The energy efficiency of formation of photons, radicals and ions during single-bubble cavitation. Nature. 2002 Jul;418(6896):394–7.
7. Brujan EA, Ikeda T, Matsumoto Y. Jet formation and shock wave emission during collapse of ultrasound-induced cavitation bubbles and their role in the therapeutic applications of high-intensity focused ultrasound. Physics in Medicine and Biology. 2005 Oct 21;50(20):4797–809.
8. Zhao S, Dong Z, Yao C, Wen Z, Chen G, Yuan Q. Liquid-liquid two-phase flow in ultrasonic microreactors: Cavitation, emulsification, and mass transfer enhancement. AIChE Journal. 2018 Apr;64(4):1412–23.
9. Brennen CE. Cavitation in medicine. Interface Focus. 2015 Oct 6;5(5):20150022.
10. Dular M, Griessler-Bulc T, Gutierrez-Aguirre I, Heath E, Kosjek T, Krivograd Klemenčič A, et al. Use of hydrodynamic cavitation in (waste)water treatment. Ultrasonics Sonochemistry. 2016 Mar;29:577–88.
11. Fedorov K, Sun X, Boczkaj G. Combination of hydrodynamic cavitation and SR-AOPs for simultaneous degradation of BTEX in water. Chemical Engineering Journal. 2021 Aug;417:128081.
12. Verhaagen B, Fernández Rivas D. Measuring cavitation and its cleaning effect. Ultrasonics Sonochemistry. 2016 Mar;29:619–28.
13. Li ZG, Liu AQ, Klaseboer E, Zhang JB, Ohl CD. Single cell membrane poration

by bubble-induced microjets in a microfluidic chip. Lab on a Chip. 2013 Mar 21;13(6):1144.

14. Pennathur S. Micro-scale turbopump blade cavitation. Massachusetts Institute of Technology; 2001.
15. Mishra C, Peles Y. Cavitation in flow through a micro-orifice inside a silicon microchannel. Physics of Fluids. 2005 Jan;17(1):013601.
16. Mishra C, Peles Y. Size scale effects on cavitating flows through microorifices entrenched in rectangular microchannels. Journal of Microelectromechanical Systems. 2005 Oct;14(5):987–99.
17. Brennen CE. Cavitation in medicine. Interface Focus. 2015 Oct 6;5(5):20150022.
18. Chowdhury SM, Abou-Elkacem L, Lee T, Dahl J, Lutz AM. Ultrasound and microbubble mediated therapeutic delivery: Underlying mechanisms and future outlook. Journal of Controlled Release. 2020 Oct;326:75–90.
19. Koşar A, Ghorbani M, Koşar SA, Sarraf SS, Farzad A, Talabazar R, et al. Fundamentals, biomedical applications and future potential of micro-scale cavitation-a review. Lab on a Chip [Internet]. 2022 Jun 14 [cited 2022 Jun 16];22(12):2237–58. Available from: https://pubs.rsc.org/en/content/articlehtml/2022/lc/d2lc00169a
20. Medrano M, Zermatten PJ, Pellone C, Franc JP, Ayela F. Hydrodynamic cavitation in microsystems. I. Experiments with deionized water and nanofluids. Physics of Fluids. 2011 Dec;23(12):127103.
21. Mossaz S, Colombet D, Ayela F. Hydrodynamic cavitation of binary liquid mixtures in laminar and turbulent flow regimes. Experimental Thermal and Fluid Science. 2017 Jan;80:337–47.
22. Podbevsek D, Colombet D, Ledoux G, Ayela F. Observation of chemiluminescence induced by hydrodynamic cavitation in microchannels. Ultrasonics Sonochemistry. 2018 May;43(September 2017):175–83.
23. Mishra C, Peles Y. Flow visualization of cavitating flows through a rectangular slot micro-orifice ingrained in a microchannel. Physics of Fluids. 2005 Nov;17(11):113602.
24. Peles Y, Mishra C. Cavitation in MicroElectroMechanical Systems (MEMS): Importance, Deviations From Conventional Scale, and Preliminary Results. In: Volume 2: Fora. ASMEDC; 2005. p. 581–6.

25. Li J, Cheng P. Bubble cavitation in a microchannel. International Journal of Heat and Mass Transfer. 2004 Jun;47(12–13):2689–98.
26. Gallo M, Magaletti F, Cocco D, Casciola CM. Nucleation and growth dynamics of vapour bubbles. Journal of Fluid Mechanics. 2020 Jan 25;883:A14.
27. Editors F, Ehlers J, Hepp K, Board E, Frisch U, Hillebrandt W, et al. <Lecture Notes in Physics (DMML).pdf>.
28. Under L, Pressure N. Liquids Under Negative Pressure. Imre AR, Maris HJ, Williams PR, editors. Liquids Under Negative Pressure. Dordrecht: Springer Netherlands; 2002.
29. Caupin F, Herbert E. Cavitation in water: a review. Comptes Rendus Physique. 2006 Nov;7(9–10):1000–17.
30. Fisher JC. The Fracture of Liquids. Journal of Applied Physics. 1948 Nov;19(11):1062–7.
31. Davitt K, Arvengas A, Caupin F. Water at the cavitation limit: Density of the metastable liquid and size of the critical bubble. EPL (Europhysics Letters). 2010 Apr 1;90(1):16002.
32. Menzl G, Gonzalez MA, Geiger P, Caupin F, Abascal JLF, Valeriani C, et al. Molecular mechanism for cavitation in water under tension. Proceedings of the National Academy of Sciences. 2016 Nov 29;113(48):13582–7.
33. Gallo M, Magaletti F, Casciola CM. Heterogeneous bubble nucleation dynamics. Journal of Fluid Mechanics. 2021 Jan 10;906:A20.
34. Atchley AA, Prosperetti A. The crevice model of bubble nucleation. J Acoust Soc Am. 1989 Sep;86(3):1065–84.
35. Strasberg M. Onset of Ultrasonic Cavitation in Tap Water. J Acoust Soc Am. 1959 Feb;31(2):163–76.
36. Atchley AA, Prosperetti A. The crevice model of bubble nucleation. J Acoust Soc Am. 1989 Sep;86(3):1065–84.
37. Mørch KA. Reflections on cavitation nuclei in water. Physics of Fluids. 2007 Jul;19(7):072104.
38. Skripov VP. Metastable liquids. John Wiley & Sons; 1974.
39. Ayela F, Cherief W, Colombet D, Ledoux G, Martini M, Mossaz S, et al. Hydrodynamic Cavitation through “Labs on a Chip”: From Fundamentals to Applications. Augier F, editor. Oil & Gas Science and Technology – Revue d’IFP

Energies nouvelles. 2017 Jul 4;72(4):19.

40. Ghorbani M, Mohammadi A, Motezakker AR, Villanueva LG, Leblebici Y, Koşar A. Energy Harvesting in Microscale with Cavitating Flows. ACS Omega. 2017 Oct 31;2(10):6870–7.
41. Hosseinpour Shafaghi A, Rokhsar Talabazar F, Zuvin M, Talebian Gevari M, Villanueva LG, Ghorbani M, et al. On cavitation inception and cavitating flow patterns in a multi-orifice microfluidic device with a functional surface. Physics of Fluids. 2021 Mar 1;33(3):032005.
42. Ghorbani M, Sadaghiani AK, Villanueva LG, Koşar A. Hydrodynamic cavitation in microfluidic devices with roughened surfaces. Journal of Micromechanics and Microengineering. 2018 Jul 1;28(7):075016.
43. Aghdam AS, Ghorbani M, Deprem G, Cebeci FÇ, Koşar A. A New Method for Intense Cavitation Bubble Generation on Layer-by-Layer Assembled SLIPS. Scientific Reports. 2019 Dec 12;9(1):11600.
44. Medrano M, Pellone C, Zermatten PJ, Ayela F. Hydrodynamic cavitation in microsystems. II. Simulations and optical observations. Physics of Fluids. 2012;24(4):47101.
45. Nayebzadeh A, Wang Y, Tabkhi H, Shin JH, Peles Y. Cavitation behind a circular micro pillar. International Journal of Multiphase Flow. 2018 Jan;98:67–78.
46. Ghorbani M, Aghdam AS, Gevari MT, Koşar A, Cebeci FÇ, Grishenkov D, et al. Facile hydrodynamic cavitation ON CHIP via cellulose nanofibers stabilized perfluorodroplets inside layer-by-layer assembled SLIPS surfaces. Chemical Engineering Journal. 2020;382:122809.
47. Stieger T, Agha H, Schoen M, Mazza MG, Sengupta A. Hydrodynamic cavitation in Stokes flow of anisotropic fluids. Nature Communications 2017 8:1. 2017 May;8(1):1–11.
48. Ghorbani M, Chen H, Villanueva LG, Grishenkov D, Koşar A. Intensifying cavitating flows in microfluidic devices with poly(vinyl alcohol) (PVA) microbubbles. Physics of Fluids. 2018 Oct;30(10):102001.
49. Mossaz S, Colombet D, Ayela F. Hydrodynamic cavitation of binary liquid mixtures in laminar and turbulent flow regimes. Experimental Thermal and Fluid Science. 2017 Jan;80:337–47.
50. Matsudaira Y, Gomi Y, Oba R. Characteristics of Bubble-Collapse Pressures in a

Karman-Vortex Cavity. JSME international journal Ser 2, Fluids engineering, heat transfer, power, combustion, thermophysical properties. 1992 May;35(2):179–85.

51. Ghorbani M, Deprem G, Ozdemir E, Motezakker AR, Villanueva LG, Kosar A. On “Cavitation on Chip” in Microfluidic Devices With Surface and Sidewall Roughness Elements. Journal of Microelectromechanical Systems. 2019 Oct;28(5):890–9.
52. Podbevšek D, Petkovšek M, Ohl CD, Dular M. Kelvin-Helmholtz instability governs the cavitation cloud shedding in Venturi microchannel. International Journal of Multiphase Flow. 2021 Sep;142:103700.
53. Ayela F, Medrano-Muñoz M, Amans D, Dujardin C, Brichart T, Martini M, et al. Experimental evidence of temperature gradients in cavitating microflows seeded with thermosensitive nanoprobes. Physical Review E. 2013 Oct 31;88(4):043016.
54. Buogo S, Cannelli GB. Implosion of an underwater spark-generated bubble and acoustic energy evaluation using the Rayleigh model. J Acoust Soc Am. 2002 Jun;111(6):2594–600.
55. Zhang LC, Zhu XL, Huang YF, Liu Z, Yan K. Development of a simple model for predicting the spark-induced bubble behavior under different ambient pressures. Journal of Applied Physics. 2016 Jul;120(4):043302.
56. Aitken F, Mcluskey FMJ, Denat A. An energy model for artificially generated bubbles in liquids. Journal of Fluid Mechanics. 1996 Nov;327:373–92.
57. Kattan R, Denat A, Lesaint O. Generation, growth, and collapse of vapor bubbles in hydrocarbon liquids under a high divergent electric field. Journal of Applied Physics. 1998 Jun;66(9):4062.
58. Buogo S, Plocek J, Vokurka K. Efficiency of energy conversion in underwater spark discharges and associated bubble oscillations: Experimental results. Acta Acustica united with Acustica. 2009 Jan;95(1):46–59.
59. Sato T, Tinguely M, Oizumi M, Farhat M. Evidence for hydrogen generation in laser- or spark-induced cavitation bubbles. Applied Physics Letters. 2013 Feb;102(7):074105.
60. Prosperetti A. The speed of sound in a gas–vapour bubbly liquid. Interface Focus. 2015 Oct 6;5(5):20150024.
61. Blake JR, Leppinen DM, Wang Q. Cavitation and bubble dynamics: the Kelvin impulse and its applications. Interface Focus. 2015 Oct;5(5):20150017.

62. Wang Q, Liu W, Zhang AM, Sui Y. Bubble dynamics in a compressible liquid in contact with a rigid boundary. Interface Focus. 2015 Oct;5(5):1–12.
63. Gevari MT, Parlar A, Torabfam M, Koşar A, Yüce M, Ghorbani M. Influence of fluid properties on intensity of hydrodynamic cavitation and deactivation of Salmonella typhimurium. Processes. 2020;8(3):326.
64. Weijs JH, Seddon JRT, Lohse D. Diffusive Shielding Stabilizes Bulk Nanobubble Clusters. ChemPhysChem. 2012 Jun;13(8):2197–204.
65. Ohgaki K, Khanh NQ, Joden Y, Tsuji A, Nakagawa T. Physicochemical approach to nanobubble solutions. Chemical Engineering Science. 2010 Feb;65(3):1296–300.
66. Hatanaka SI, Mitome H, Yasui K, Hayashi S. Single-Bubble Sonochemiluminescence in Aqueous Luminol Solutions. Journal of the American Chemical Society. 2002 Sep;124(35):10250–1.
67. Tandiono, Ohl SW, Ow DSW, Klaseboer E, Wong V V, Dumke R, et al. Sonochemistry and sonoluminescence in microfluidics. Proceedings of the National Academy of Sciences. 2011 Apr;108(15):5996–8.
68. Podbevsek D, Colombet D, Ledoux G, Ayela F. Observation of chemiluminescence induced by hydrodynamic cavitation in microchannels. Ultrasonics Sonochemistry. 2018 May;43(September 2017):175–83.
69. Podbevšek D, Colombet D, Ayela F, Ledoux G. Localization and quantification of radical production in cavitating flows with luminol chemiluminescent reactions. Ultrasonics Sonochemistry. 2021 Mar;71:105370.
70. Perrin L, Colombet D, Ayela F. Comparative study of luminescence and chemiluminescence in hydrodynamic cavitating flows and quantitative determination of hydroxyl radicals production. Ultrasonics Sonochemistry. 2021 Jan;70(June 2020):105277.
71. Koşar A, Şeşen M, Oral O, Itah Z, Gozuacik D. Bubbly cavitating flow generation and investigation of its erosional nature for biomedical applications. IEEE Transactions on Biomedical Engineering. 2011 May;58(5):1337–46.
72. Perk OY, Şeşen M, Gozuacik D, Koşar A. Kidney stone erosion by micro scale hydrodynamic cavitation and consequent kidney stone treatment. Ann Biomed Eng [Internet]. 2012 Sep 3 [cited 2022 Jun 13];40(9):1895–902. Available from: http://www.ncbi.nlm.nih.gov/pubmed/22476893

73. Itah Z, Oral O, Perk OY, Sesen M, Demir E, Erbil S, et al. Hydrodynamic cavitation kills prostate cells and ablates benign prostatic hyperplasia tissue. Experimental Biology and Medicine [Internet]. 2013 Nov 18 [cited 2022 Jun 13];238(11):1242–50. Available from: http://journals.sagepub.com/doi/10.1177/1535370213503273

74. Uzusen D, Demir E, Perk OY, Oral O, Ekici S, Unel M, et al. Assessment of probe-to-specimen distance effect in kidney stone treatment with hydrodynamic cavitation. Journal of Medical Devices, Transactions of the ASME [Internet]. 2015 Sep 1 [cited 2022 Jun 13];9(3). Available from: https://asmedigitalcollection.asme.org/medicaldevices/article/9/3/031001/448110/Assessment-of-Probe-to-Specimen-Distance-Effect-in

75. Ghorbani M, Oral O, Ekici S, Gozuacik D, Kosar A. Review on Lithotripsy and Cavitation in Urinary Stone Therapy. IEEE Reviews in Biomedical Engineering [Internet]. 2016 [cited 2022 Jun 13];9:264–83. Available from: http://ieeexplore.ieee.org/document/7479522/

76. Sozer C, Ghorbani M, Alcan G, Uvet H, Unel M, Kosar A. Design, Prototyping and Control of a Flexible Cystoscope for Biomedical Applications. IOP Conference Series: Materials Science and Engineering [Internet]. 2017 Jul 1 [cited 2022 Jun 13];224(1):012050. Available from: https://iopscience.iop.org/article/10.1088/1757-899X/224/1/012050

77. Ghorbani M, Sozer C, Alcan G, Unel M, Ekici S, Uvet H, et al. Biomedical device prototype based on small scale hydrodynamic cavitation. AIP Advances [Internet]. 2018 Mar 8 [cited 2022 Jun 13];8(3):035108. Available from: http://aip.scitation.org/doi/10.1063/1.5005048

78. Gevari MT, Aydemir G, Gharib G, Kutlu O, Uvet H, Ghorbani M, et al. Local Carpet Bombardment of Immobilized Cancer Cells With Hydrodynamic Cavitation. IEEE Access [Internet]. 2021 [cited 2022 Jun 13];9:14983–91. Available from: https://ieeexplore.ieee.org/document/9328434/

79. Abbasiasl T, Sutova H, Niazi S, Celebi G, Karavelioglu Z, Kirabali U, et al. A Flexible Cystoscope Based on Hydrodynamic Cavitation for Tumor Tissue Ablation. IEEE Transactions on Biomedical Engineering [Internet]. 2022 Jan 1 [cited 2022 Jun 13];69(1):513–24. Available from: https://ieeexplore.ieee.org/document/9502580/

80. Spray formation under the effect of micro scale cavitation and its biomedical applications - Sabanci University Research Database [Internet]. [cited 2022 Jun 18]. Available from: https://research.sabanciuniv.edu/id/eprint/41481/
81. Rokhsar Talabazar F, Sheibani Aghdam A, Jafarpour M, Grishenkov D, Koşar A, Ghorbani M. Chemical effects in “hydrodynamic cavitation on a chip”: The role of cavitating flow patterns. Chemical Engineering Journal. 2022 Oct 1;445:136734.
82. Rokhsar Talabazar F, Jafarpour M, Zuvin M, Chen H, Gevari MT, Villanueva LG, et al. Design and fabrication of a vigorous “cavitation-on-a-chip” device with a multiple microchannel configuration. Microsystems & Nanoengineering 2021 7:1 [Internet]. 2021 Jun 2 [cited 2021 Sep 30];7(1):1–13. Available from: https://www.nature.com/articles/s41378-021-00270-1
83. Abbasiasl T, Niazi S, Aghdam AS, Chen H, Cebeci FÇ, Ghorbani M, et al. Effect of intensified cavitation using poly(vinyl alcohol) microbubbles on spray atomization characteristics in microscale. AIP Advances [Internet]. 2020 Feb 12 [cited 2021 Sep 30];10(2):025318. Available from: https://aip.scitation.org/doi/abs/10.1063/1.5142607
84. Podbevšek D, Petkovšek M, Ohl CD, Dular M. Kelvin-Helmholtz instability governs the cavitation cloud shedding in Venturi microchannel. International Journal of Multiphase Flow. 2021 Sep 1;142:103700.
85. Bachmann A, Ruszat R. The KTP-(greenlight-) laser – principles and experiences. http://dx.doi.org/101080/13645700601157885 [Internet]. 2009 [cited 2022 Jun 23];16(1):5–10. Available from: https://www.tandfonline.com/doi/abs/10.1080/13645700601157885
86. Kanagawa T, Kamei T. Thermal effect inside bubbles for weakly nonlinear pressure waves in bubbly liquids: Theory on short waves. Physics of Fluids. 2021 Jun;33(6):063319.
87. Johnsen E, Colonius T. Numerical simulations of non-spherical bubble collapse. Journal of Fluid Mechanics. 2009;629:231–62.
88. Zupanc M, Kosjek T, Petkovšek M, Dular M, Kompare B, Širok B, et al. Shear-induced hydrodynamic cavitation as a tool for pharmaceutical micropollutants removal from urban wastewater. Ultrasonics Sonochemistry. 2014 May;21(3):1213–21.

89. Stewart MP, Sharei A, Ding X, Sahay G, Langer R, Jensen KF. In vitro and ex vivo strategies for intracellular delivery. Nature 2016 538:7624. 2016 Oct;538(7624):183–92.
90. Stewart MP, Langer R, Jensen KF. Intracellular Delivery by Membrane Disruption: Mechanisms, Strategies, and Concepts. Chemical Reviews. 2018 Aug;118(16):7409–531.
91. Stewart MP, Langer R, Jensen KF. Intracellular Delivery by Membrane Disruption: Mechanisms, Strategies, and Concepts. Chemical Reviews. 2018 Aug;118(16):7409–531.
92. Chen D, Sun Y, Gudur MSR, Hsiao YS, Wu Z, Fu J, et al. Two-Bubble Acoustic Tweezing Cytometry for Biomechanical Probing and Stimulation of Cells. Biophysical Journal. 2015 Jan;108(1):32–42.
93. Li F, Yang C, Yuan F, Liao D, Li T, Guilak F, et al. Dynamics and mechanisms of intracellular calcium waves elicited by tandem bubble-induced jetting flow. Proceedings of the National Academy of Sciences. 2018 Jan 16;115(3):E353–62.
94. Li F, Yuan F, Sankin G, Yang C, Zhong P. A Microfluidic System with Surface Patterning for Investigating Cavitation Bubble(s)–Cell Interaction and the Resultant Bioeffects at the Single-cell Level. Journal of Visualized Experiments. 2017 Jan 10;2017(119):e55106.
95. Stewart MP, Sharei A, Ding X, Sahay G, Langer R, Jensen KF. In vitro and ex vivo strategies for intracellular delivery. Nature [Internet]. 2016 Oct 12 [cited 2022 Feb 6];538(7624):183–92. Available from: http://www.nature.com/articles/nature19764
96. Bailey MR, Khokhlova VA, Sapozhnikov OA, Kargl SG, Crum LA. Physical mechanisms of the therapeutic effect of ultrasound (a review). Acoustical Physics 2003 49:4. 2003 Jul;49(4):369–88.
97. Ghorbani M, Oral O, Ekici S, Gozuacik D, Kosar A. Review on Lithotripsy and Cavitation in Urinary Stone Therapy. IEEE Reviews in Biomedical Engineering. 2016;9:264–83.
98. Engelberger RP, Kucher N. Ultrasound-assisted thrombolysis for acute pulmonary embolism: a systematic review. European Heart Journal. 2014 Mar;35(12):758–64.
99. Weiss HL, Selvaraj P, Okita K, Matsumoto Y, Voie A, Hoelscher T, et al.

Mechanical clot damage from cavitation during sonothrombolysis. J Acoust Soc Am. 2013 May;133(5):3159.

100. Dixon AJ, Li J, Rickel JMR, Klibanov AL, Zuo Z, Hossack JA. Efficacy of Sonothrombolysis Using Microbubbles Produced by a Catheter-Based Microfluidic Device in a Rat Model of Ischemic Stroke. Annals of Biomedical Engineering. 2019 Jan;47(4):1012–22.
101. Kim H, Kim J, Wu H, Zhang B, Dayton PA, Jiang X. A multi-pillar piezoelectric stack transducer for nanodroplet mediated intravascular sonothrombolysis. Ultrasonics. 2021 Sep;116:106520.
102. Gong M, Chen G, Zhao B, Kong J, Gu J, He X. Rescue catheter-based therapies for the treatment of acute massive pulmonary embolism after unsuccessful systemic thrombolysis. Journal of Thrombosis and Thrombolysis. 2021 Apr;51(3):805–13.
103. Perk OY, Şeşen M, Gozuacik D, Koşar A. Kidney stone erosion by micro scale hydrodynamic cavitation and consequent kidney stone treatment. Annals of Biomedical Engineering. 2012;40(9):1895–902.
104. Itah Z, Oral O, Perk OY, Sesen M, Demir E, Erbil S, et al. Hydrodynamic cavitation kills prostate cells and ablates benign prostatic hyperplasia tissue. Experimental Biology and Medicine. 2013;238(11):1242–50.
105. Abbasiasl T, Sutova H, Niazi S, Celebi G, Karavelioglu Z, Kirabali U, et al. A Flexible Cystoscope Based on Hydrodynamic Cavitation for Tumor Tissue Ablation. IEEE Transactions on Biomedical Engineering. 2022 Jan;69(1):513–24.